MSc Thesis

Evaluating GFS analysis and forecast data for pest and disease modelling

author:
Sippora Stellingwerf

August 4, 2017

supervisor:
Oscar Hartogensis

Abstract

In many developing countries there are no systems for alarming farmers of the risk of plant diseases and insect pests. The growth, and therefore risk of plant diseases and pests are mainly related to weather conditions. Insects require an accumulation of heat, while diseases are also dependant on sufficient moisture availability. The relationships between meteorological variables and the development of insects and plant diseases are used in simple, species-specific models. Unfortunately, in most developing countries meteorological observations, used as input in such models, are lacking or of questionable quality. I have investigated whether an alternative source of meteorological data are suitable: the analysis and forecast data from the Global Forecast System (GFS) from the National Centres for Environmental Predictions. In areas with a strong topography temperature and relative humidity are highly variable in space. In such areas the spatial resolution of the GFS data are too coarse for obtaining localised risk indices. Therefore I have applied and validated several methods to downscale the GFS data to a kilometre scale level, methods which are based on a high resolution Digital Elevation Model. To validate the downscaling methods, I have made use of an extensive observational network in Washington State (USA). I have then analysed how sensitive insect en disease models are to the quality of the meteorological data. I have shown that using downscaled data significantly improves insect pest prediction compared to using uncorrected GFS data. However, GFS data are less suitable for predicting disease risk due to the systematic underestimation of relative humidity in cropland areas.

Contents

1 Introduction **3**

2 Data description **5**
2.1 Site and meteorological network description 5
2.2 Quality check of meteorological stations 8
2.3 GFS analysis and forecast dataset 9

3 Methodology **11**
3.1 Spatial downscaling of analysis data 11
3.1.1 Temperature 11
3.1.2 Relative humidity and pressure 14
3.2 Insect and disease models 15
3.2.1 Insects 15
3.2.2 Diseases 17
3.3 Statistical model validation 19

4 Results **19**
4.1 GFS 2 m Temperature 19
4.1.1 GFS performance without downscaling 19
4.1.2 GFS performance with downscaling 25
4.2 GFS 2 m Relative humidity 32
4.2.1 GFS performance without downscaling 32
4.2.2 GFS performance with downscaling 34
4.3 Insect modelling 34
4.4 Disease modelling 37

5 Discussion **39**

6 Conclusion **41**

7 Acknowledgements **43**

Bibliography **43**

1 Introduction

In many developing countries insect pests and plant diseases can cause major economical damages to the agricultural sector (Food and of the United Nations, 2001). Farmers are usually solely dependent on their own knowledge and experience concerning the mitigation of these hazards. An example is the department of Santa Cruz, Bolivia. With 13% of Bolivia's Gross Domestic Product originating from agriculture and 32% of Bolivians' occupations related to agriculture (Central Intelligence Agency, 2015), the agricultural sector is of major importance to the country of Bolivia. With an estimated 45% of the population living below the poverty line of $2/day (Central Intelligence Agency, 2015) successful harvests are essential. However, structural pest and disease monitoring is lacking and plagues may come without warning, causing harvest losses.

Fortunately, several simple models are available that predict the development of plant diseases and insects as their growth largely depends on atmospheric conditions (Rosenzweig et al., 2001). Insects for example require a certain amount of accumulated heat to be able to develop and are thus dependent on air temperature (Ludwig, 1928). Plant diseases, on the other hand, are more complex and require, depending on the species, a certain humidity, air temperature, duration of leaf wetness and/or precipitation (West et al., 2012). Combining these relationships with meteorological data as input these models can keep track of the current pest and disease risk and predict the timing of organisms' developmental stages. For example, an insect model may indicate when insect eggs start hatching. The larvae may then feed on, and damage, crops. This is necessary information for farmers to know the right timing for applying pest management. More advanced insect and disease models exist (e.g. Sankaran et al. (2010); Tonnang et al. (2017)) but will not be treated in this thesis, as they require more advanced, localised input data.

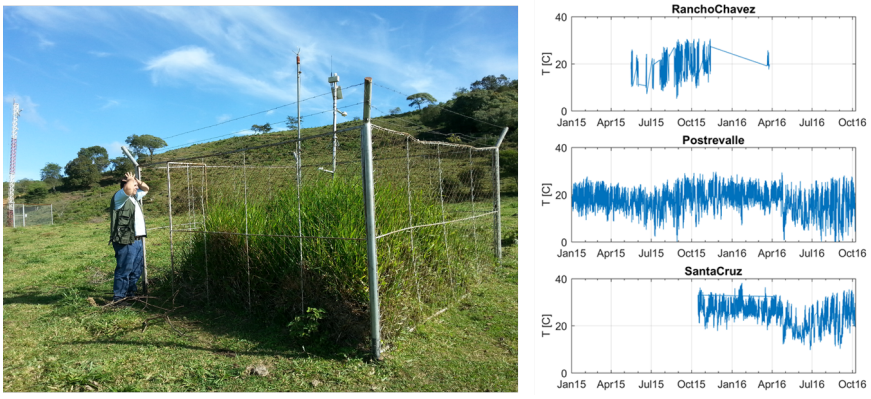

Figure 1: Example of how stations in developing countries may be of questionable quality due to a lack of maintenance. Left: A meteorological station which is partly overgrown by uncut grass. Right: An example of air temperature data from three stations, some of which show large gaps. All examples shown are from meteorological stations in Santa Cruz, Bolivia.

The general idea of simple insect pest and disease models is quite straightforward, but there is one major problem. In many developing regions, such as Bolivia, the required meteorological observations to feed these models are scarce. Even if they are present they might be of insufficient quality (Figure 1). Financial resources to maintain stations might be lacking, which inhibits a continuous data provision. Concluding, there is a need for providing meteorological data which does not depend on the presence of local meteorological observations.

In this study I will investigate whether the output from General Circulation Models (GCM) can be used as an alternative source for meteorological data for pest and disease modelling. Every day GCMs assimilate observational data from extensive sources worldwide. These are then used to create an analysis and forecast dataset completely covering the Earth, consisting of fields of various meteorological variables. I will use the analysis and forecast dataset of the National Centres for Environmental Prediction (National Centers for Environmental Prediction, 2015), which is created with the Global Forecast System (GFS). This dataset is freely available and accessible world-wide, which makes it especially attractive for application in developing regions.

Using the output from GFS, or any GCM model as is, may however not always be suitable for agricultural use. Currently, GFS is available on a horizontal resolution of 0.25 x 0.25 degrees. However, in areas with a strong topography weather is spatially very heterogeneous and this resolution may not be sufficient for application on the field, for which information on a localised, kilometre-scale level would be much more suitable (Figure 2).

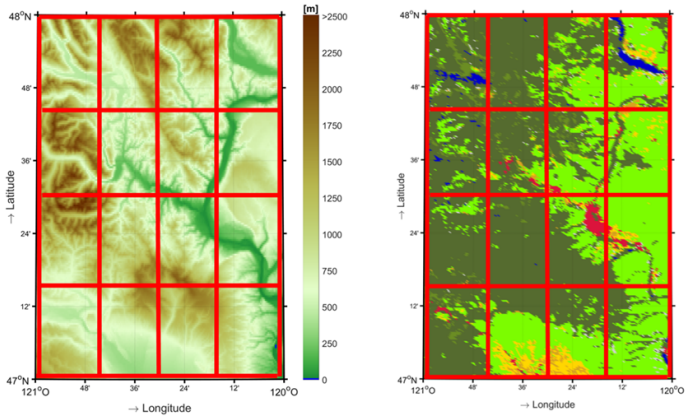

Figure 2: Example of the spacial heterogeneity of elevation (left) and land use (right, specific land use categories not shown). The grid in red represents the resolution of the GFS data.

Therefore, the first step of my research will be to spatially downscale the GFS data using a high resolution Digital Elevation Model. Downscaling temperature based on elevation is done using a lapse rate which describes the change of temperature with height. Often, these lapse rates are fixed at -6.5 °C/km (Lundquist and Cayan, 2007; Maurer et al., 2002; Stahl et al., 2006). However, using the

vertical temperature profile that is incorporated within GFS may give a better estimation of the true lapse rate, as it may vary with time and space. In this thesis, several methods for defining this model-internal lapse rate will be implemented and used to downscale temperature and, related to that, relative humidity. The downscaled GFS data will be validated using an extensive meteorological network in Washington State (USA), an area which hosts the Cascade mountain range. Finally, I will evaluate pest and disease models using downscaled GFS data and see if the downscaled GFS data are of sufficient quality to be used on a field-scale level. My prime motivation of this thesis is to help farmers in Santa Cruz, Bolivia, gain resilience to insect pests and diseases, but the research done in this thesis could be applied in mountainous areas worldwide. I divide my research into the following research questions:

1. *How can coarse analysis and forecast data be downscaled to a local, kilometre scale level?*
2. *How do downscaled data compare to observations?*
3. *How sensitive are disease and pest models to the accuracy of the meteorological data input?*

This thesis first describes the data sources in Chapter 2. I will elaborate on how to use this data to answer my research questions in Chapter 3. The results are presented and discussed in Chapter 4. I will then provide an overarching discussion and put my results into perspective in Chapter 5 and draw conclusions based on my research in Chapter 6.

2 Data description

2.1 Site and meteorological network description

To validate downscaled analysis and forecast data I made use of an extensive meteorological network situated in Washington State in the mountainous North-West of the USA. The Cascade mountain range divides the state in the two distinct regions: a mild, marine western Washington and a dry, continental eastern Washington (Figure 3). The main large-scale weather pattern is characterised by prevailing westerly winds that transport moisture into the marine west of Washington and precipitates out on the wind-ward slopes of the mountains. This leaves relatively warm and dry air to reach the Columbian plateau in eastern Washington. Average annual rainfall is extremely variable and ranges from approximately 5000 mm (200 inches) near the highest mountain peaks to 200 mm (8 inches) in the driest areas in the Columbian plateau (Figure 3).

The meteorological network in Washington State is maintained by AgWeatherNet (WSU, 2017). Variables measured include air temperature, relative humidity, pressure, wind, rainfall, soil moisture and temperature, solar incoming radiation and leaf wetness. Not every station measures all of these components, though air temperature is always included. To ensure continuous air temperature data, each stations has two thermometers incorporated, usually the Rotronic HC2S3 and a Campbell 107 temperature probe. In total I used meteorological data of 165 stations for the whole year of 2016. The data have a

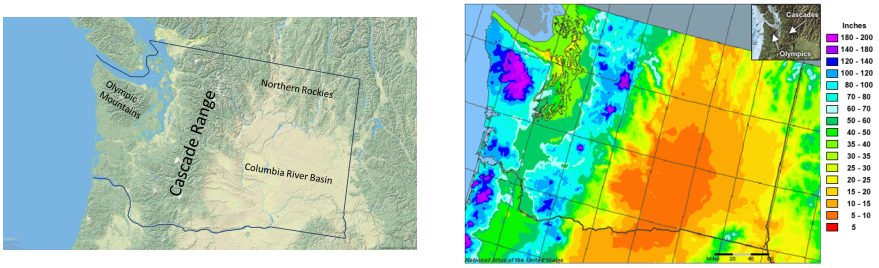

Figure 3: Left: Topographical map of Washington State, main topograpic units are displayed (Google Earth, 2017). Right: Map showing average annual precipitation in inches in Washington State from 1961-1990 (UCAR, 2017)

.

temporal resolution of 15 minutes which are produced from averaging 5-second readings over a 15-minute window. I downsampled this data to a 3-hourly resolution in order to validate the 3-hourly GFS data. Most weather stations are located in valley positions, in or near agricultural fields (Figure 4 and 5).

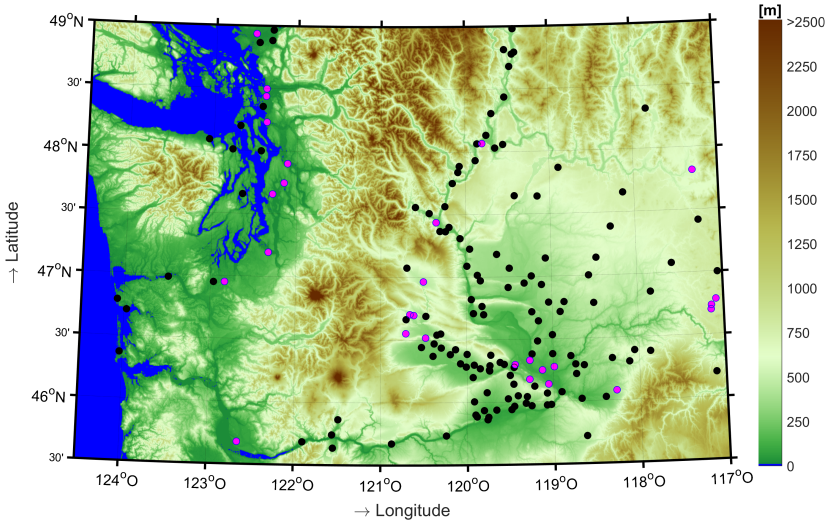

Figure 4: Elevation map for Washington State, with elevation in meters above sea level. The dots denote the locations of meteorological stations. The magenta dots denote stations that did not pass the quality check (Section 2.2).

The Digital Elevation Model (DEM) I used in this study is the ASTER Global Digital Elevation Model (NASA JPL, 2009). This DEM covers the entire earth with a 30 m pixel size. The elevation in Washington State ranges from sea level to 4392 m a.s.l., the height of the highest mountain of the state: Mount Rainier (Figure 4). To obtain detailed information on the elevation of the meteorological stations, the DEM is slightly upscaled to a resolution of 1.8" (approximately

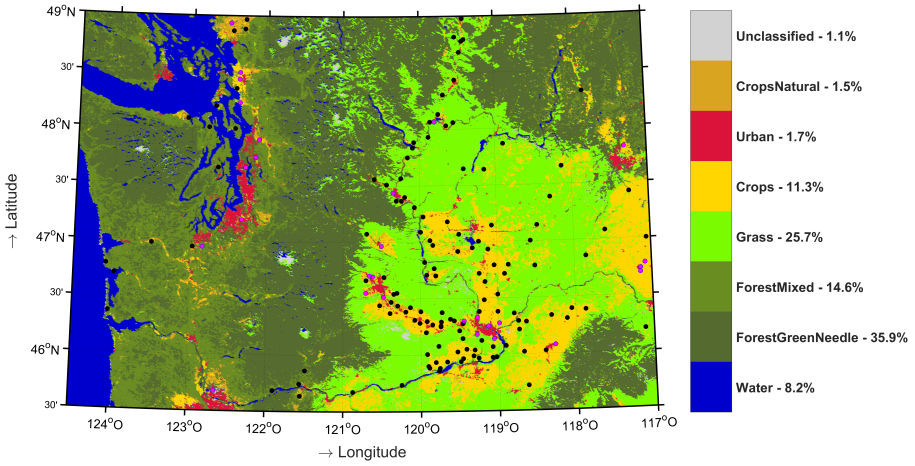

Figure 5: Land Cover map of Washington State. The legend shows abbreviated land use classifications in subsequent order: Unclassified, Cropland/natural vegetation mosaic, Urban and built-up, Croplands, Grasslands, Mixed forest, Evergreen Needleleaf forest and Water. The dots denote the locations of meteorological stations. The magenta dots denote stations that did not pass the quality check (Section 2.2).

50 meridional metres).

The land use map used in this thesis is the MODIS Land Cover map (Friedl et al., 2010). I used the most recent, 2012 land cover dataset with a spatial resolution of 5' x 5', approximately 0.083 degrees or roughly 9 x 9 km. A large part of Washington State, mainly the marine region to the west and the mountainous areas, is covered by forests. The Columbian Plateau in the East is intensively used for agriculture, with interconnected crop fields and pivots that extend up to tens of kilometres in length. The agricultural area is mostly surrounded by (dry) grasslands. Vancouver to the South-West and Seattle in the North-West are the main urban areas and smaller cities can be found mostly on the Columbian Plateau (Figure 5).

2.2 Quality check of meteorological stations

First, I will discuss the data reliability of the meteorological stations followed by the effect of urban areas on the temperature.

All stations are equipped with two thermometers. If the temperatures recorded by both thermometers differ too much from each other, the data are considered unreliable. These data are not used for validation. To filter out unreliable data I performed a systematic quality check for each station, per day and per month. The daily and monthly filters are applied in order to validate on a daily and seasonal basis.

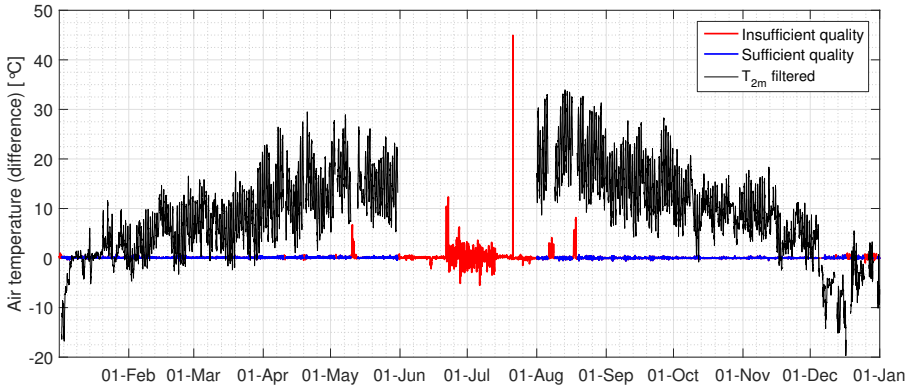

Figure 6: Example of data filtering for station WSU Othello. Red and blue: Air temperature$_1$ - Air temperature$_2$, with red the data that is labelled as unreliable. Black: The resulting air temperature data that passed the quality test.

First, a daily quality check was done, with the following criteria for filtering out unreliable data:

- At least 10% of the measurements show a difference between the temperature of thermometer 1 and thermometer 2 of more than 0.5 °C.
- There is at least one instance where the difference in temperatures is larger than 1 °C.
- One or more measurements are missing.

If during a day one or more of the criteria is met, the whole day is filtered out and every measurement is replaced with a dummy value. Hereafter, a monthly quality check was done, with the following criterion:

- At least 10 days fully consist of dummy values.

If this criterion is met, the temperature measurements of the whole month is replaced with dummy values. This ensures that for a monthly validation sufficient reliable observations are present. An example of the data filtering is given in Figure 6. For pressure and relative humidity such data filtering is not possible, as for each of these variables there is only one measuring device. However,

pre-existing dummy values within the dataset are not used for validation. Next to checking the reliability of temperature readings using the aforementioned filtering procedure, I left out stations which are located within or near urban areas.

Urban areas are sensitive to the urban heat island (UHI) effect. Compared to the surrounding rural areas cities are warmer, especially during night (Oke, 1982). As the spatial resolution of the GFS model may not always be sufficient for incorporating the UHI effect, the modelled temperatures will in general be too low (Figure 7). As the error caused by the UHI is dominant over the error due to elevation differences I did not use stations in or near urban areas for the validation process. For selecting such stations I used the USGS land cover map described earlier. 11 stations were labelled as urban in de land cover map and 15 stations were in close proximity to urban or built areas.

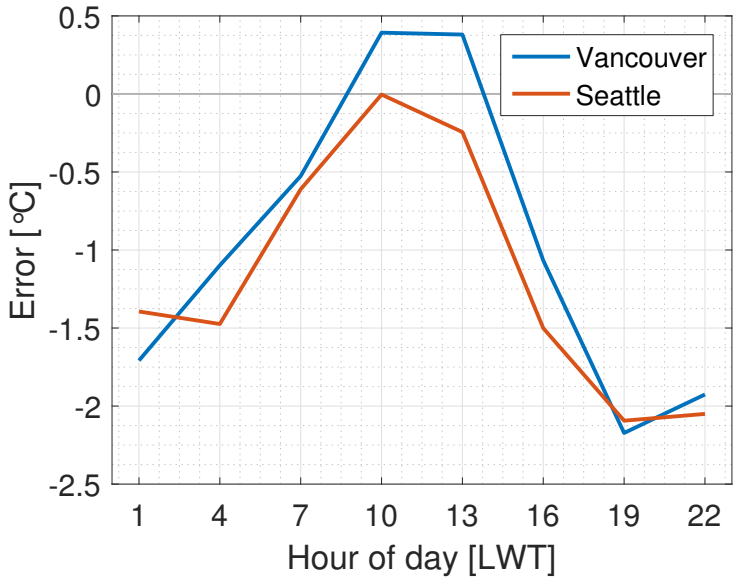

Figure 7: Bias error ($T2m_{GFS} - T2m_{obs}$) throughout the day, averaged for 2016, for two exemplary urban stations: Seattle and Vancouver. The hour of day is given in Local Winter Time (LWT). I adjusted for elevation difference using a lapse rate of -6.5 °C/km.

Next to the 26 urban or near-urban stations, 2 stations did not fulfil the quality criteria throughout the whole year of 2016, leaving 137 stations for validation.

2.3 GFS analysis and forecast dataset

I investigated whether analysis and forecast data of a General Circulation Model (GCM) can substitute for meteorological observations and subsequently be used for insect and disease modelling. The analysis and forecast dataset I used is the NCEP GDAS/FNL (Final) 0.25 Degree Global Tropospheric Analyses and Forecast Grids dataset ds083.3 (National Centers for Environmental Prediction, 2015). This dataset is created using the same model as the Global Forecast

System (GFS) but it is initialised one hour later in order to incorporate approximately 10% more observational data (Peng, 2015). As a consequence the final analyses are somewhat delayed but provide the most realistic global analysis.

The analysis and forecast dataset has a temporal coverage starting July 2015 and is archived until a near-current date, approximately until 5 days to the current date. For every 6 hours, in addition to an analysis, a 3-, 6-, and 9-hour forecast is made. I will make use of the 6-hourly analyses and the accompanied +3 hour forecasts for obtaining a dataset with a temporal resolution of 3 hours. The spatial resolution is 0.25 by 0.25 degrees and covers the entire globe. A full description of the dataset can be found on NCEP's website (National Centers for Environmental Prediction, 2015). In the remainder of this thesis I refer to this dataset using GFS as an abbreviation.

3 Methodology

3.1 Spatial downscaling of analysis data

In heterogeneous areas plant pest and disease models are most effective when providing output on a local, kilometre-scale. However, the GFS data have a relatively coarse horizontal resolution of 0.25 x 0.25 degrees that cannot capture local, field-scale variability. To overcome this problem I will downscale the GFS analysis and forecast data. In simple insect and disease models temperature is the most important variable. Next to temperature, relative humidity can play an important role for disease modelling. In the following I will discuss methodologies for downscaling these variables as well as pressure, which is needed to downscale relative humidity. For validating the downscaling techniques, I downscale GFS data to a resolution of approximately 50 m and only to the sub-grids in which meteorological stations are located. This will minimize errors caused by the uncertainty of the elevation of a station and reduce computational power and memory.

3.1.1 Temperature

Air temperature decreases with height. Using the air temperature of the GFS grid cell and combining this with high resolution elevation data, using a certain lapse rate, the GFS data can be downscaled to a sub-grid level. After defining a lapse rate, Γ, the temperature at sub-grid i, j, having a specific elevation, follows from Equation 1:

$$T_{i,j} = T_{GFS} + \Gamma \times \Delta z_{i,j} \tag{1}$$

With T_{GFS} being the GFS analysis temperature [°C], Γ being the lapse rate [°C/km] and $\Delta z_{i,j}$ being the difference in height [km] between the sub-grid i, j and the GFS grid, thus:

$$\Delta z_{i,j} = z_{i,j} - z_{GFS} \tag{2}$$

For defining the lapse rate several methodologies exist. The easiest and fastest way is to define a fixed lapse rate. A commonly used lapse rate is -6.5 °C km^{-1} (Lundquist and Cayan, 2007; Maurer et al., 2002; Stahl et al., 2006). This does not account for spatial, nor for temporal variability of the lapse rate. Another approach is to compute a lapse rate by interpolating temperature measurements at varying elevations (Stahl et al., 2006). This is however not a realistic option for regions with no or scarce observations. A more complex method which accounts for both spatial and temporal variation in the lapse rate is to use the GCM-internal lapse rate, as has been done with the ERA-Interim reanalysis dataset by Gao et al. (2012). He showed that using a model-internal lapse rate reduced the root-mean-square error by 32% compared to when using a literature-based, monthly lapse rate.

To obtain a model-internal lapse rate one must choose upper and lower isobaric levels of which the difference in temperature and geopotential height are used according to Equation 3.

$$\Gamma = \frac{T_{up} - T_{low}}{gph_{up} - gph_{low}} \tag{3}$$

With T_{up} and T_{low} being the temperature [°C] at the upper and lower boundary of the chosen atmospheric layer defined by gph_{up} and gph_{low} [km]. For every grid cell and for every 3 hours, the GFS dataset consists of vertical pressure levels of which temperature and geopotential height are modelled.

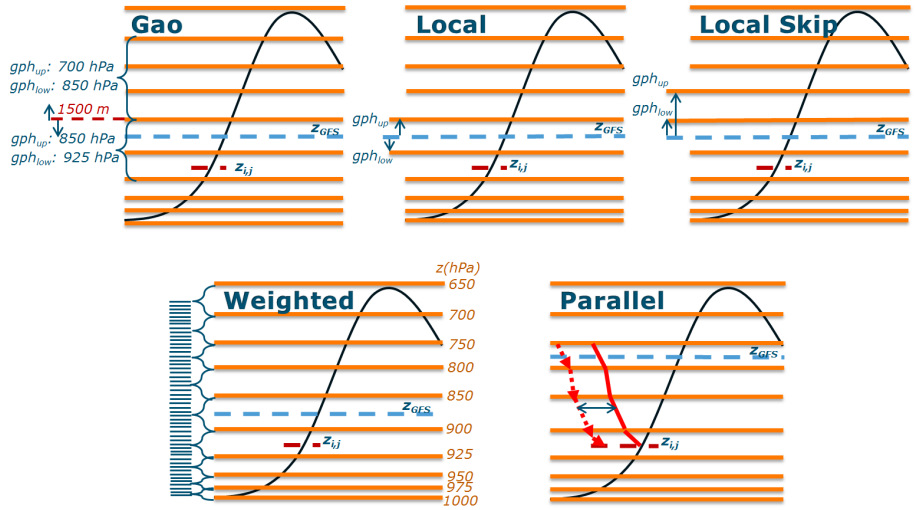

Figure 8: Schematic representation of the different methods used for defining a model-internal lapse rate. The lapse rate is obtained from the temperature and geopotential height at certain pressure levels (orange lines, specific levels are depicted for the Weighted method only but the same levels apply for each method). Using the model-internal lapse rate the GFS 2 m temperature at the height of the GFS grid (z_{GFS}) is downscaled to the temperature the height of the sub-grid ($z_{i,j}$).

I will evaluate several methods for using the GFS temperature profile and geopotential heights to calculate model-internal lapse rates. Next to using model-internal lapse rates (Figure 8), I will test the usage of a fixed lapse rate. All downscaling methods are summarised in Table 1. The Fixed and Gao method are based on literature, whereas the subsequent methods are novel methods introduced in this study. In the following the methods are discussed in more detail.

Fixed

The first method is to simply use a spatio-temporally fixed lapse rate of -6.5 °C/km.

Gao

The second method is based on Gao et al. (2012) and is therefore simply referred to as the Gao method. Gao separates the atmosphere into two layers that are controlled by two different processes. Down in the valley, Gao assumes the atmosphere to be mostly controlled by a local circulation pattern, whereas aloft the atmospheric flow can be described by a free air flow. He makes this

Table 1: Summarised description of the methods for defining a lapse rate.

Method	Description
Fixed	Lapse rate fixed at -6.5 °C/km
Gao	$z_{i,j} < 1500 \rightarrow gph_{up}$: 850 hPa; gph_{low}: 925 hPa $z_{i,j} > 1500 \rightarrow gph_{up}$: 700 hPa; gph_{low}: 850 hPa
Local	First GFS pressure level above and below z_{GFS}
Local Skip	As Local, but lower and upper level move one level vertically upwards
Parallel	Use GFS' $T_{profile}(2m)$ and interpolate to $z_{i,j}$. Maintain bias $T_{2m} - T_{profile}(2m)$
Weighted	Interpolate all layers of the T_{prof} from 650 to 1000 hPa to sublayers of $\Delta z = 50m$ and calculate the lapse rate for every sub-layer. Sort lapse rates and calculate mean of the interquartile range

separation at 1500 m a.s.l., approximately the geopotential height of the 850 hPa pressure level. Based on the sub-grid elevation, $z_{i,j}$, he then calculates either a 'free atmospheric' or 'local' lapse rate. If the sub-grid is located lower than 1500 m a.s.l., gph_{up} and gph_{low} are set to 850 and 925 hPa respectively. If the sub-grid is located higher than 1500 m a.s.l, gph_{up} and gph_{low} are set to 700 and 850 hPa respectively.

Local
The first novel method, Local, was defined to assess the effect of using only a shallow atmospheric layer of the GFS temperature profile to define a localised lapse rate. This method uses the first GFS pressure level above and below the height of the GFS grid, z_{GFS} as the upper and lower boundary, respectively.

Local Skip
The fourth method, Local Skip, is the same as Local, however the upper and lower level are shifted one level upwards. The idea behind this method is to not incorporate pressure levels that are located below the GFS surface. The GFS model calculates a temperature profile down to 1000 hPa even in mountainous regions where surface pressure is always lower. If, for example, the upper and lower level for a certain sub-gird as defined by the Local method are 750 and 700 hPa, the upper and lower level for the Local Skip method are 700 and 650 hPa.

Parallel
The fifth method, Parallel, makes use of the vertical temperature profile of GFS ($T_{prof,GFS}$) and linearly interpolates the profile to the sub-grid elevation $z_{i,j}$. The lapse rate itself is thus not explicitly calculated. The 2 m temperature of GFS may not always coincide with the temperature of the profile interpolated to 2 m above the GFS surface. This bias, $T_{2m} - T_{profile}(2m)$, is maintained. The most likely reason for this bias is that surface processes are incorporated in the calculations of the GFS 2 m temperature, but not in the vertical temperature profile. The vertical temperature profile represents a modelled state of the atmosphere if no topography were present, whereas the 2 m temperature is

calculated incorporating surface processes and maintaining the surface energy balance.

Weighted
The last method, Weighted, makes use of the whole atmospheric layer that comprises the elevation range of Washington State (except for the two highest mountain peaks). Opposite to the Local methods, here I used a broad atmospheric layer to calculate a weighted lapse rate, from 650 hPa down to 1000 hPa. These levels are fixed regardless of the elevation of the GFS grid. In reality the surface of a GFS grid may be located above the 1000 hPa pressure level. Despite this, these levels are fixed in order not to introduce uncertainties in the validation of this method that originate from a variable layer from which the lapse rate is calculated.

The vertical temperature profile from 650 to 1000 hPa is interpolated to sub-layers with a Δz of 50 m. For each of the sub-layer a lapse rate is calculated. The resulting weighted lapse rates are then sorted based on their magnitudes and the final lapse rate is calculated from the mean of the interquartile range, i.e. all lapse rates between the 25th and 75th percentile. This is to ensure that outliers do not influence the eventual lapse rate.

3.1.2 Relative humidity and pressure

To downscale relative humidity (RH), I assume the specific humidity q [$\mathrm{kg}_v/\mathrm{kg}_d$] to be conserved. This is true if no diabatic processes or changes in air mass occur. RH at height $z_{i,j}$ can be calculated from pressure and temperature. As I assume q to remain constant, q at 2 m can be directly obtained from the GFS dataset, while the pressure and temperature at the sub-grid are obtained by downscaling. For a complete derivation of the following equations I refer to Moene and van Dam (2014).

First, the pressure at the height of a sub-grid, $p_{i,j}$ [Pa], is calculated by applying Equation 4:

$$p_{i,j} = p_{GFS} e^{-g\Delta z_{i,j}/R<T>} \tag{4}$$

With g the acceleration due to gravity [9.81 m s^{-2}], temperature $< T >$ taken as the average temperature of the considered column ($= \frac{T_{GFS}+T_{i,j}}{2}$) in [K] and p_{GFS} the GFS surface pressure [Pa]. Then, the saturated water vapour pressure, e_s [Pa] at temperature $T_{i,j}$, is obtained from Equation 5:

$$e_s(T_{i,j}) = 611.2 \exp\left[\frac{17.62(T_{i,j} - 273.15)}{-30.03 + T_{i,j}}\right] \tag{5}$$

The water vapour pressure $e_{i,j}$ [Pa] can be obtained by rewriting Equation 6:

$$q_{i,j} = q_{GFS} = \frac{\rho_v}{\rho} = \frac{R}{R_v}\frac{e_{i,j}}{p_{i,j}} \approx \frac{R_d}{R_v}\frac{e_{i,j}}{p_{i,j}} \tag{6}$$

With ρ being the total air density [kg m^{-3}], ρ_v the water vapour density [kg m^{-3}] and R the specific gas constant [J kg^{-1} K^{-1}], with subscript d and v for dry air and water vapour respectively. As $q \ll 1$, $R \approx R_d$. Using the downscaled

e_s and e from Equation 5 and 6, the relative humidity at height $z_{i,j}$ is calculated from Equation 7.

$$RH_{i,j} = 100 \times \frac{e_{i,j}}{e_s(T_{i,j})} \tag{7}$$

3.2 Insect and disease models

3.2.1 Insects

Insects are ectotherm organisms, meaning their internal temperature is the same as their surroundings. Throughout the life cycle of an insect, from egg to larva, from larva to pupa and finally egg-laying adults insects are dependant on heat to grow. For example, when the temperature is below a species-specific threshold, a hibernating pupa will not yet evolve to its adult form. When the temperature exceeds the lower threshold the growth rate generally increases linearly with temperature. Depending on the species above a certain temperature the growth rate does not increase anymore, perhaps slows down or even ceases.

The heat accumulation required to fulfil a certain life stage has shown to be fairly constant per species (Bursell, 1964). Keeping track of the air temperature allows one to predict fairly well the timing of certain developmental stages. Knowledge on the current status of an organism's development is crucial for successfully timing pest management.

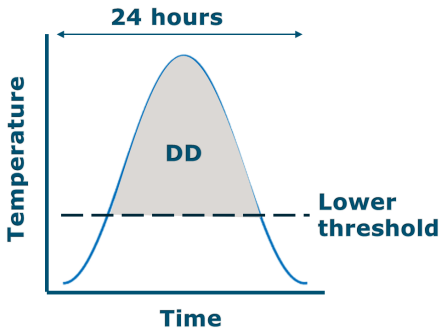

Figure 9: The concept of degree day accumulation. Degree days (in grey) are accumulated when the temperature exceeds a certain minimum temperature threshold. (Adapted from University of California (2016))

Using temperature data as input the aforementioned concept is used to define simple insect models. These empirical models are based on species-specific heat accumulations required for completing developmental stages. The specific heat accumulations have been found from conducting lab experiments and are usually validated in one or multiple regions.

Heat accumulation is expressed as a unit of temperature times a unit of time. Often, degree days (DD) are used. When the temperature is above the lower threshold by 1 degree for 24 hours, 1 DD has been accumulated. This concept is visualised in Figure 9. The start date to keep tracking the degree day ac-

cumulation differs per model. Some models simply start accumulating degree days on a fixed calendar date, other models start accumulating when a 'bio-fix' occurs, e.g. the first time an insect has been spotted in the field, or caught in a trap.

In some insect models not only a lower temperature threshold is defined, but an upper threshold as well. Different methodologies exist for defining how temperatures exceeding the upper threshold affect population growth. These so-called cut-off methods are shown in Figure 10. If an insect model assumes growth to remain constant after exceeding the upper threshold a horizontal cut-off is applied. The growth rate is then no longer increasing with increasing temperature, nor does the growth rate decrease. Insect populations may also be affected negatively by temperatures exceeding the upper threshold. If at too high temperatures the growth rate slows down, an intermediate cut-off is applied. For some insects, too high temperatures may even be fatal and cease growth completely. Then, a vertical cut-off is used.

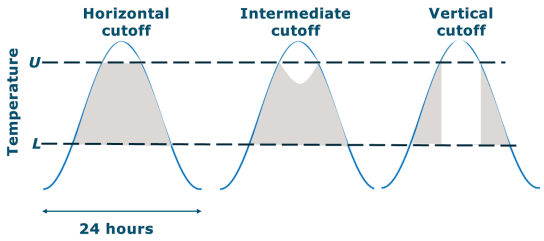

Figure 10: Different cut-off methods. (Adapted from University of California (2016))

In this research I have used one exemplary insect model to assess the applicability of downscaled GFS temperature for insect modelling: the Western cherry fruit fly. Ali Niazee (1979) experimentally obtained a model which provides the amount of degree days that are required to fulfil developmental stages (Table 2). The Western cherry fruit fly requires a temperature of at least 5 °C in order to develop. In this model, there is no upper temperature limit for development. The degree day accumulation starts on a fixed calender date, March 1.

Table 2: Degree-day accumulations required for each stage of development of the Western cherry fruit fly. The degree days are accumulated from March 1 onwards. (Ali Niazee, 1979)

Stage	DD (°C×day)
First adult spring emergence	462
Beginning of egg-laying	541
Egg hatch	594
50% adult spring emergence	631
Peak egg-laying	685
Pupation	795

3.2.2 Diseases

Plant diseases are caused by viral, bacterial or fungal pathogens. Contrary to insect development the growth and spread of pathogens is more complex and is influenced not only by temperature, but often by (relative) humidity, rainfall and/or leaf wetness duration as well (University of California, 2016; West et al., 2012). Typically, the relative humidity has to be high enough (e.g. $> 90\%$) for a plant disease to develop.

As an exemplary disease model, I will use an adapted model of Ullrich and Schrödter (1966) for Late Blight on potatoes. This model calculates a weekly risk of Late Blight using hourly data of temperature and relative humidity. For every week the hour sum when relative humidity requirements are met are multiplied by a multiplication factor which depends on temperature. All multiplied hour sums are then added up to generate a weekly risk value. If the risk value exceeds 150 disease is expected (Table 3). This adapted model, contrary to the original, does not contain a rainfall requirement.

The model shows two peaks for the multiplication factor, one around 11 degrees and one around 21 degrees. This bi-modal behaviour stems from the optimal temperature which is lower for germination and infection on the one hand, and higher for pathogen growth on the other hand. The range of temperatures Late Blight requires for development is between 9 and 24 °C. The risk for blight increases when the period of consecutively high relative humidity is longer. During unfavourable conditions of low relative humidity, the risk decreases.

Table 3: Adapted Late Blight model (Ullrich and Schrödter, 1966). The risk for Late Blight is calculated per week based on hourly relative humidity and temperature data. For every week the hour sum (h) when certain requirements (right column) are met combined with a certain temperature range (middle column) is multiplied by a multiplication factor (r, left column). The resulting 14 $r \times h$ values are then summed to obtain a weekly risk value. If the risk value exceeds 150 disease is expected.

Multiplication factor (r)	Number of hours hourly temperature averages are in this range (h), or other conditions to be met	RH requirements, or other conditions to be met
0.899	10.0 - 11.9	Only count hours that co-occur with 4 or more consecutive hours at RH>=90%.
0.4118	14.0 - 15.9	
0.5336	16.0 - 17.9	
0.8816	18.0 - 19.9	
1.0498	20.0 - 21.9	
0.5858	22.0 - 23.9	
0.3924	10.0 - 11.9	Only count hours that co-occur with 10 or more consecutive hours at RH>=90%.
0.0702	14.0 - 15.9	
0.1278	16.0 - 17.9	
0.9108	18.0 - 19.9	
1.4706	20.0 - 21.9	
0.855	22.0 - 23.9	
0.1639	15.0 - 19.9	Do not consider RH or rain, add 7.5479 to the product of r x h
0.0468	Number of hours with average RH $< 70\%$	Subtract 7.8624 from the product of r $\times$ h

3.3 Statistical model validation

For statistically validating the model results against data from meteorological stations I have made use of two difference measures: The root-mean-square error ($RMSE$) and the bias error. Whereas the bias gives a good indication of a systematic error, the $RMSE$ is used to assess the performance of downscaling methods. If elevation differences between the meteorological station and the GFS grid are dominant in determining the error, the subsequent systematic cold or warm bias will be corrected for after downscaling. This will then reduce the bias error as well as the $RMSE$. In the following, O refers to the observed variate obtained from the meteorological stations, while P refers to the GFS model-predicted variate. The $RMSE$ is calculated from:

$$RMSE = [N^{-1} \sum_{i=1}^{N} (P_i - O_i)^2]^{0.5} \tag{8}$$

The bias error is calculated from:

$$Bias = N^{-1} \sum_{i=1}^{N} (P_i - O_i) \tag{9}$$

4 Results

This chapter presents this research's results and interpretation. First, I will discuss the uncorrected and downscaled GFS 2 meter temperature in Section 4.1 and the 2 meter relative humidity in Section 4.2. As this concerns validation only, GFS data was only downscaled to sub-grids which contain meteorological stations. Except when explicitly stated, stations that did not pass the quality test, the urban stations as well as two unreliable stations, were not used for obtaining the following results.

Finally, the use of either observed, uncorrected and downscaled weather data for insect and disease modelling will be discussed in Section 4.3 and 4.4.

4.1 GFS 2 m Temperature

The GFS 2 m air temperature is downscaled to the elevation of a sub-grid by applying adiabatic warming or cooling following a certain lapse rate. The performance of GFS when no downscaling is applied is assessed in Section 4.1.1. First, the area as a whole is considered after which the focus shifts to stations with $|\Delta z_{i,j}| < 30$ m. For these stations, errors are hardly influenced by elevation differences. This is followed by the performance of GFS when downscaling is applied in Section 4.1.2. As the downscaling methods are based on elevations differences, the methods are validated using only stations with $|\Delta z_{i,j}| > 100$ m. For these stations, elevation differences are relatively more important in determining the bias of GFS.

4.1.1 GFS performance without downscaling

First I will discuss the overall performance of the GFS model, considering all meteorological stations for the whole year 2016. This includes urban as well

as two unreliable stations. Before applying downscaling methods, the spatio-temporal mean of the $RMSE$ of the GFS 2 m temperature is 2.5 °C, with a standard deviation (σ) of 0.7 °C. This is the mean of all 165 meteorological stations over the whole year of 2016.

However, the $RMSE$ varies with space and time. The spatial variation of the time-averaged $RMSE$ can be seen in Figure 11. The lowest accuracy, or highest $RMSE$, can be found in mountainous areas with a strong topography (mean $RMSE$: 3.5 °C). This is to be expected as large elevation differences will cause rapid spatial temperature differences. Nevertheless, also areas with a relatively weak topography, the marine lowlands in the west (mean $RMSE$: 2.0 °C) and the stations on the Columbian Plateau (mean $RMSE$: 2.3 °C) show considerable errors which may partly be related to land-use related effects.

It was to be expected that a strong topography will cause a high $RMSE$. Indeed, for stations positioned relatively high in the landscape (high meaning higher than the GFS grid elevation), GFS overestimates the 2 m temperature and vice versa (Figure 12). However, for each station the bias shows a significant temporal variation as indicated by the error bars. The temporal bias variation can have several explanations: the performance of the GFS model is not constant throughout time, cooling or warming due to local phenomena are time-dependant (e.g. irrigation during the growing season), the lapse rate is not constant, but variable in time or other processes are present that determine the error. Literature on the upper air climatology of the United States already show a seasonal variation of lapse rate (Kunkel (1988) and Ratner (1957)) with higher (drier) lapse rates in summer and lower (more moist) lapse rates in winter. These climatological lapse rates and the observed lapse rates in Washington State are plotted in Figure 13. The seasonal variation of the lapse rate in Washington State shows a similar behaviour compared to the literature-based climatology, however the summer pattern is distinctly different. This is likely to be explained by irrigation, which will be further elaborated upon in the Discussion.

The variability of the GFS performance is assessed using the temperature observations from stations with a $|\Delta z_{i,j}| < 30$ m. For these stations errors are hardly caused by elevation differences. In total, 31 such stations exist. These stations show a similar land use distribution compared to the land use distribution of all stations, regardless of the station elevation (Figure 14). This ensures that the stations selected to assess the performance of the GFS model are representative for the whole observational network used to assess the downscaling methods. Note that the land use distribution of the meteorological stations in general is not the same as the land use distribution of the area as a whole (Figure 14). As the observation network is used mostly for agricultural purposes, the stations are biased to being located in the vicinity of crop fields.

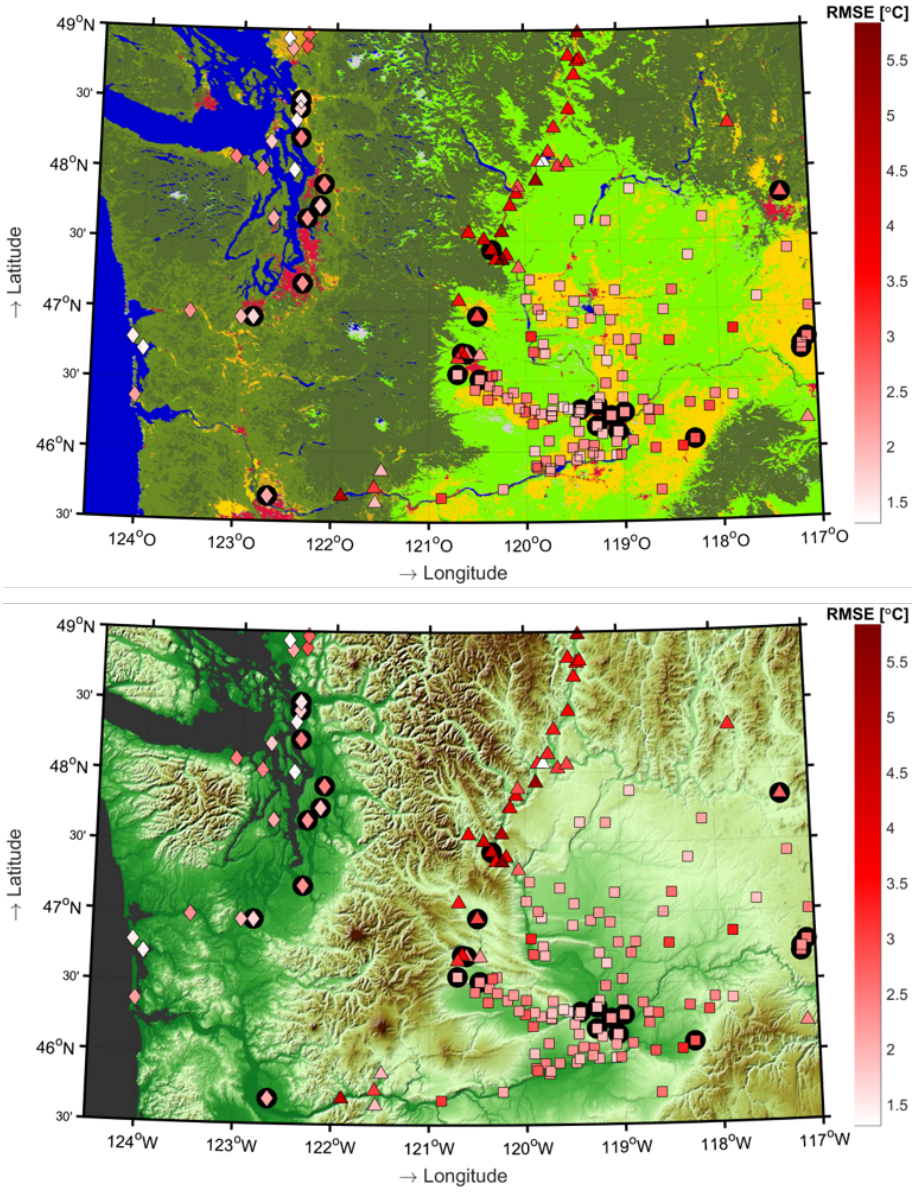

Figure 11: The time-averaged $RMSE$ of the GFS 2 m temperature before applying downscaling methods. Upper panel: Background of the land use map; lower panel: Background of the DEM. The symbols denote the sub-area: diamonds for marine stations, triangles for mountainous stations and squares for stations in the Columbian Plateau. Black circles denote stations that are classified as Urban and built up, or are situated in the vicinity of urban areas. All 165 stations are incorporated in this figure, including the 28 stations that did not pass the quality test.

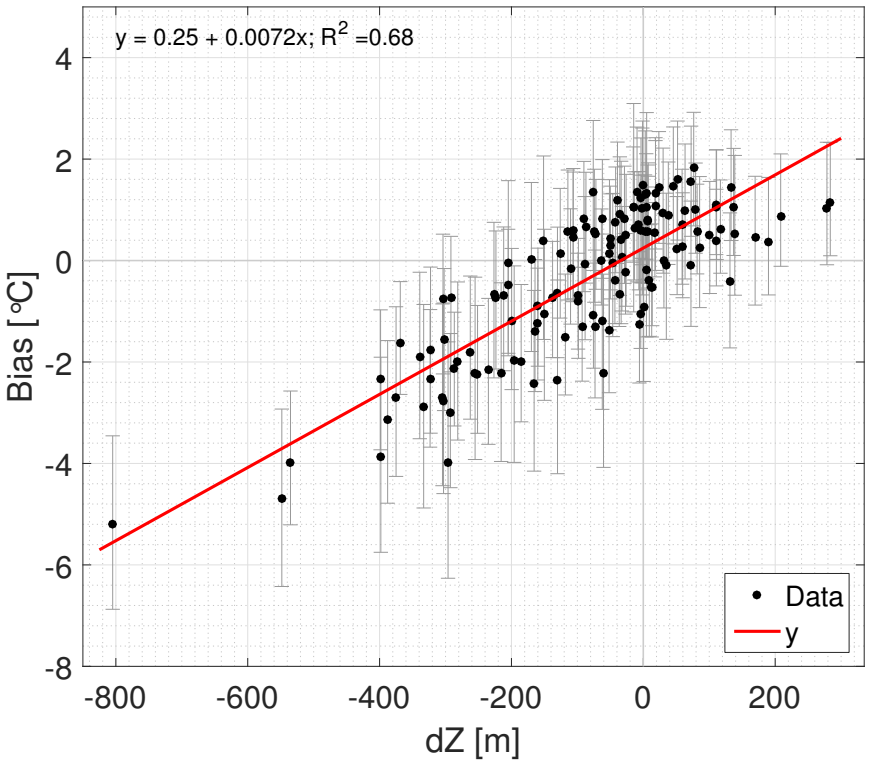

Figure 12: Mean bias error ($T2m_{GFS} - T2m_{obs}$) for each station (black dots) versus $\Delta z_{i,j}$ (=elevation station - elevation GFS). The error as a function of $\Delta z_{i,j}$ is computed using simple linear regression with intercept (y). The error bars indicate the 25th and the 75th percentile of the error throughout 2016. Urban stations are not included, as well as 2 stations of poor quality, leaving 137 stations.

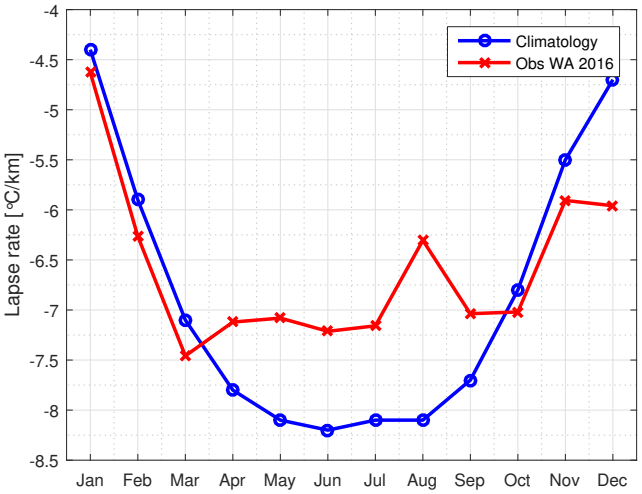

Figure 13: Temporal variability of the adiabatic lapse rate. Red: Observed monthly lapse rates for Washington State. These were obtained by applying simple linear regression to the stations' monthly bias versus their $\Delta z_{i,j}$, interpreting the regression slope as the lapse rate, similar to the slope of y in Figure 12. Stations used were non-urban and had an absolute value for $\Delta z_{i,j}$ larger than 100 m. Blue: Climatology of lapse rates for the United States, calculated by Kunkel (1988) from upper-air measurements from Ratner (1957).

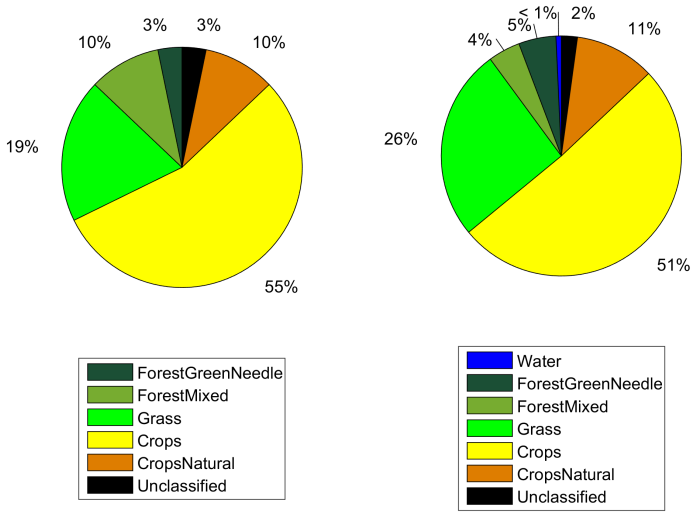

Figure 14: Land use distribution for stations used to assess the temporal performance of GFS, with an absolute $\Delta z_{i,j}$ smaller than 30 m (left) and the land use distribution of all stations (right). Note that urban stations are not used for assessing the GFS model performance, and are thus not shown in these pie charts.

Figure 15 shows the temporal variability of the bias of GFS separately for cropland and non-cropland stations. Even though $\Delta z_{i,j}$ is too small to matter (a super-adiabatic lapse of -10 °C would at most cause a 0.3 degree bias) there is a significant bias between the model and observation. In general, the model overestimates the 2 m temperature, especially for cropland stations. A clear exception is 16 LWT, when on average hardly any bias is present. This may however be caused by known a deficiency in the GFS model: the rapid decoupling of the boundary layer after sunset, followed by a too rapid cool-down (*Personal communication with Grace Peng, NCEP*). During night the spread of the bias is large for non-cropland stations but consistently warm for cropland stations. Throughout the year, the warm bias is strongest in summer for cropland stations whereas December and January show a slight cold bias regardless of land use type. This will be discussed in Section 5.

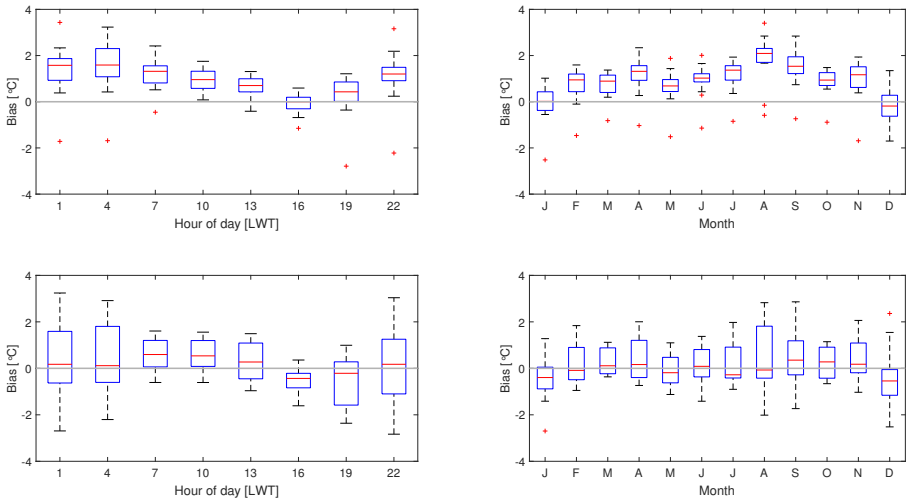

Figure 15: Bias ($T2m_{GFS} - T2m_{obs}$) for stations with $|\Delta z_{i,j}| < 30$ m. The hour of day is given in Local Winter Time (LWT). For each box, the central mark is the median, the edges are the 25th and 75th percentile and the whisker includes all points not considered outliers. Data beyond approximately 2.7 standard deviations from the median are considered outliers and denoted with red '+'-symbols. All data, including outliers, are shown.

4.1.2 GFS performance with downscaling

I have validated the downscaled GFS data against stations with a $|\Delta z_{i,j}| > 100$ m. This is done because for these stations elevation differences play a dominant role in the systematic bias of GFS. The performance of the different methods is assessed using only those instances when, for a given time step, all methods give a realistic lapse rate, realistic defined as $-10 < \Gamma - 3$. To ensure a fair comparison the statistics are based on model output when all methods provide a realistic lapse rate simultaneously. All sample sizes are in this way equal. Similarly, the original, uncorrected GFS data are used for the statistics only when all lapse rates are realistic. In this way, also the sample size for the uncorrected GFS data is equal to those of the downscaling methods. This ensures that any reduction in $RMSE$ is solely caused by downscaling, and not by a decrease in sample size. Spatially averaged, realistic lapse rates are calculated simultaneously during 45% of the time. First, I will assess the performance of the downscaling methods based on the reduction in $RMSE$ with respect to the uncorrected GFS data. I will do this separately for stations with a $\Delta z_{i,j} > 100$ m and subsequently for stations with a $\Delta z_{i,j} < -100$ m. One should keep in mind that the GFS model is already biased towards warmer temperatures, most clearly during daytime and in the summer months (Figure 15).

Using stations with a $\Delta z_{i,j} > 100$ m, the daily and yearly variation of $RMSE$ for uncorrected and downscaled GFS data is given in Figure 16. For these sub-grids, the GFS 2 m temperature is adiabatically cooled. Throughout the day, downscaling is most effective in the morning and the early afternoon with a $RMSE$ reduction of approximately 0.5 °C. During these hours, GFS performs relatively well and shows a slight warm bias (see Figure 15). As GFS performs better during day, elevation differences will become more dominant in determining the bias. In addition, the slight warm bias (also Figure 15) makes the adiabatic cooling extra effective. Due to the 16 LWT cool bias, downscaling only slightly decreases the $RMSE$. At night, the $RMSE$ reduction is less significant, or even slightly increasing (19 LWT). Throughout the year, downscaling is most effective during spring and autumn, while for the summer months the reduction is lower. In December and January, the already present cold bias is increased by adiabatic cooling. This further increases the $RMSE$ when applying downscaling. This is likely to be caused by irrigation and snow coverage, which will be discussed in Section 5. When 'going up', applying downscaling reduces the $RMSE$ by 12 to 15% (Table 4). The differences among downscaling methods are small. The Parallel method is most effective when 'going up'.

Using stations with a $\Delta z_{i,j} < -100$ m, the daily and yearly variation of $RMSE$ for uncorrected and downscaled GFS data is given in Figure 17. When going down, the air is warmed adiabatically. Interestingly, downscaling is now more effective during night than during day. During day, the already warm bias is aggravated by applying adiabatic warming. Apparently, the pre-existing warm bias is stronger than a cold bias caused by elevation differences. During night, for sub-grids with $\Delta z_{i,j} < -100$ m there is on average a strong cold bias (not shown). This is effectively reduced by applying downscaling. However, even after adiabatic warming GFS still shows a night-time cold bias for around half of the stations, regardless of land-use. For these sub-grids GFS exaggerates

night-time cooling. This may be caused by the too rapid de-coupling of the boundary layer after sunset that the GFS model produces. Throughout the year all methods decrease the $RMSE$, except for the month of August. Likely, this originates from irrigation. When 'going down', applying downscaling reduces the $RMSE$ by 15 to 18% (Table 5). The differences among downscaling methods are small. The Fixed method is most effective when 'going up'.

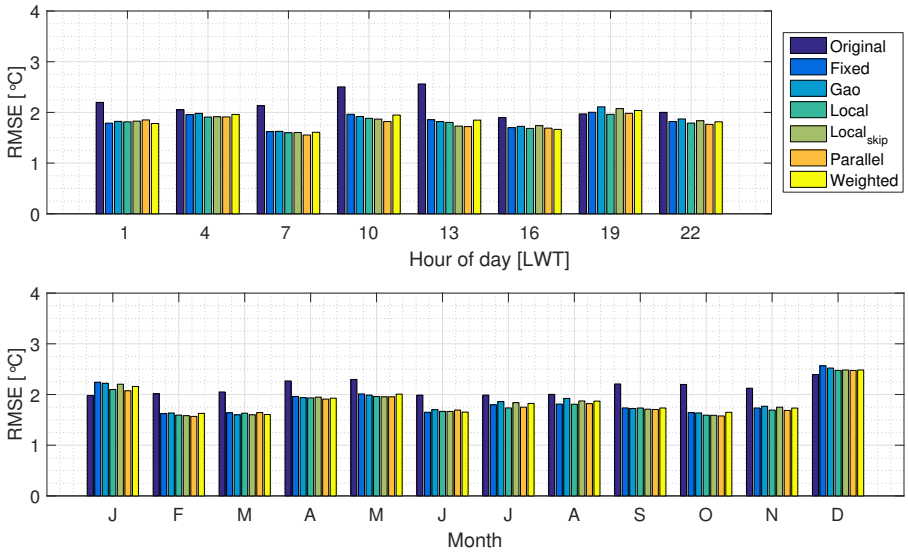

Figure 16: The $RMSE$ for the original and downscaled 2 m temperatures throughout the day (upper figure, hour of day in given in Local Winter Time (LWT)) and throughout the year (lower figure), assessed for stations with $\Delta z_{i,j} > 100$ m. For these stations, the average $\Delta z_{i,j}$ is equal to 159 m.

Table 4: $RMSE$ of the 2 m temperature before (Original) and after applying downscaling, and $RMSE$ reduction compared to the original $RMSE$. Assessed for stations with $\Delta z_{i,j} > 100$ m.

Method	**RMSE (°C)**	**RMSE red. (%)**
Original	2.16	-
Parallel	1.83	15.2
Local	1.84	14.7
Weighted	1.86	13.5
Fixed	1.87	13.4
Local Skip	1.87	13.3
Gao	1.90	12.1

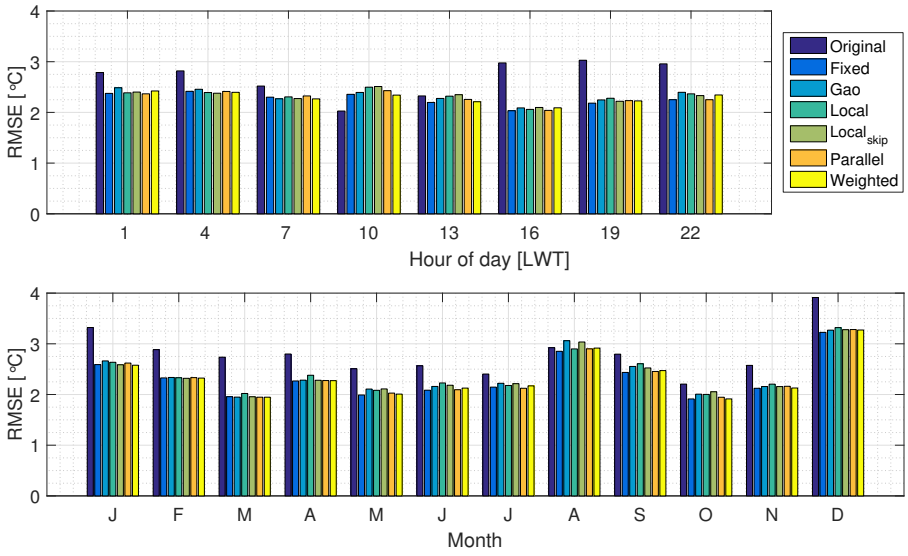

Figure 17: The $RMSE$ for the original and downscaled 2m temperatures throughout the day (upper figure, hour of day in given in Local Winter Time (LWT)) and throughout the year (lower figure), assessed for stations with $\Delta z_{i,j} < -100$ m. For these stations, the average $\Delta z_{i,j}$ is equal to -258 m.

Table 5: $RMSE$ of the 2 m temperature before (Original) and after applying downscaling, and RMSE reduction compared to the original $RMSE$. Assessed using stations with $\Delta z_{i,j} < -100$ m.

Method	RMSE (°C)	RMSE red. (%)
Original	2.93	-
Fixed	2.39	18.2
Weighted	2.42	17.4
Parallel	2.42	17.3
Gao	2.44	16.6
Local Skip	2.45	16.5
Local	2.48	15.4

Downscaling reduces the $RMSE$, both when adiabatically going upwards and downwards. Differences between downscaling methods, only looking at $RMSE$ reduction, were no larger than a few percent. The aforementioned statistics were only based on those instances when all methods provide realistic lapse rates. When calculated lapse rates are unrealistic, in practice they will be set to a fixed number, for example lapse rates >-3 °C/km can be set to -3, and rates <-10 °C/km to -10. Another option is to fix the lapse rate to -6.5 °C/km. If one has to adjust the lapse rate often, the method is not very robust. The robustness of each method can be quantified by calculating how often the lapse rate is unrealistic. This is calculated using only the stations with $|\Delta z_{i,j}| > 100$ m. The results are shown in Table 6. The Local Skip method is the least robust, only in 63% of the time it gives realistic lapse rates. The Weighted method has the highest occurrence of realistic lapse rates, after the Fixed method, which has a prescribed lapse rate and is therefore always robust.

When the methods do give realistic lapse rates, the mean lapse rates among different methods do not differ too much (Table 7). The Gao method produces the strongest lapse rate, whereas the Weighted methods calculates on average the weakest lapse rate. When focussing on lapse rate variability the Local Skip method produces the most variable lapse rates. The reason for this is that the local methods only use a thin layer of the atmosphere to calculate the lapse rate. Over short distances the profile may be erratic and the lapse rate fluctuating rapidly. On the other hand the Weighted method is, among the model-internal lapse rates, the least variable. This method takes a much larger part of the vertical profile into account and calculates a smartly weighted lapse rate.

Table 6: Overall percentage of occurrences each method generates a realistic lapse rate, realistic defined as being in between -10 and -3 °C/km.

Method	Mean occurrence (%)	Standard deviation (%)
Fixed	100	0
Weighted	97	1
Parallel	86	17
Gao	79	9
Local	77	16
Local Skip	63	11

Table 7: The average and standard deviation of the generated lapse rates when methods provide a realistic lapse rate, realistic defined as being in between -10 and -3 °C/km.

Method	Mean lapse rate (°C/km)	Std (°C/km)
Weighted	-6.3	1.3
Fixed	-6.5	0
Parallel	-6.5	1.6
Local	-6.6	1.6
Local Skip	-6.7	2.1
Gao	-6.9	1.9

The Weighted method effectively reduces the $RMSE$ while being both variable (through space and time) and robust. Therefore, I consider the Weighted method to be most suitable for downscaling temperature. Before downscaling 68% of the temperature bias could be explained by $\Delta z_{i,j}$ ($R^2 = 0.68$, Figure 12). After downscaling the temperature bias is no longer related to $\Delta z_{i,j}$, which shows from the small regression coefficient and R^2 value (Figure 18). Before downscaling, the GFS warm bias, which can be deducted from the intercept, was 0.25 °C. This warm bias is not related to $\Delta z_{i,j}$ and thus remains practically unchanged.

The Weighted method will be used to downscale relative humidity in Section 4.2. The downscaled temperature and relative humidity using the Weighted method will be applied for insect and disease modelling in Section 4.3 and 4.4 respectively.

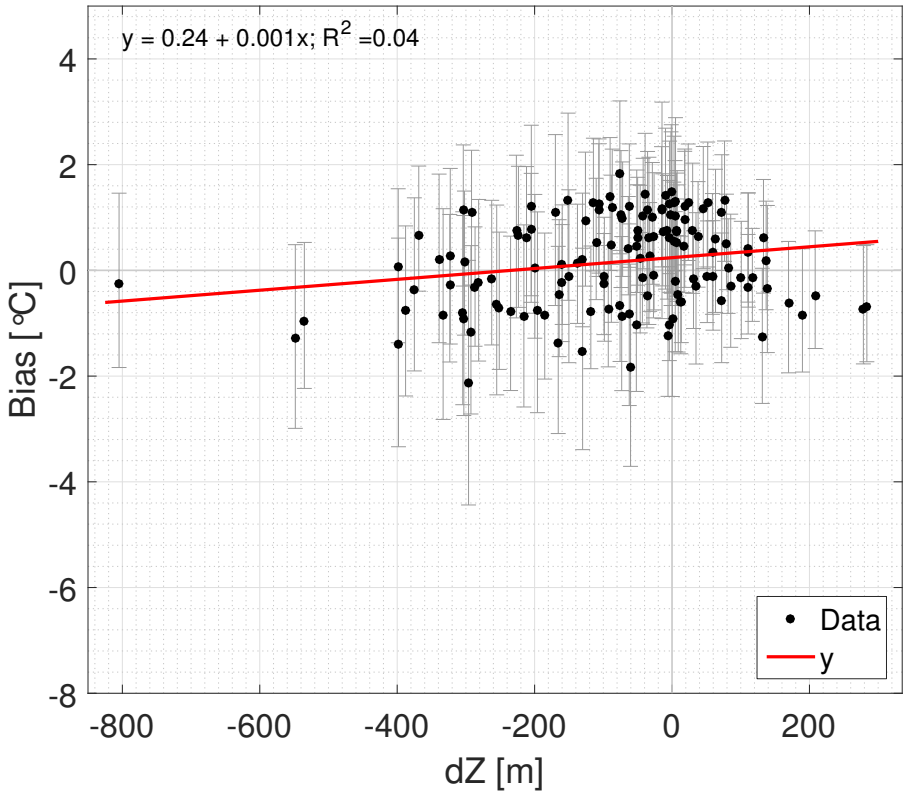

Figure 18: Mean bias error ($T2m_{GFS} - T2m_{obs}$) for each station (black dots) versus $\Delta z_{i,j}$ after downscaling using the Weighted method. The error as a function of $\Delta z_{i,j}$ is computed using simple linear regression with intercept (y). The error bars indicate the 25th and the 75th percentile of the error throughout 2016. Urban stations are not included, as well as 2 stations of poor quality, leaving 137 stations.

4.2 GFS 2 m Relative humidity

Before downscaling the GFS 2 m relative humidity (RH) in Section 4.2.2, I will first assess the performance of GFS 2 m RH in Section 4.2.1. The focus is first laid upon the validation of uncorrected GFS data against all stations (except urban and unreliable stations). Then the focus shifts specifically to the GFS performance assessed using stations with a $|\Delta z_{i,j}| < 30$. The downscaling methods are finally validated using all stations.

Often disease models require hourly relative humidity input, therefore the following analysis is based on GFS 3-hourly relative humidity data that has been linearly interpolated to 1-hourly data. The use of non-downscaled, downscaled and observed relative humidity for disease modelling will be discussed in 4.4.

4.2.1 GFS performance without downscaling

Relative humidity is related to temperature and decreases with increasing temperature (keeping the specific humidity constant). It is to be expected that relative humidity is overestimated when the GFS temperature has a cold bias, as cold air can contain less water vapour and vice versa. The bias of relative humidity versus $\Delta z_{i,j}$ is given in Figure 19. It can be seen that indeed the bias of relative humidity is, through temperature, related to $\Delta z_{i,j}$. What first strikes the eye is that, for all stations, GFS underestimates the relative humidity, which can be seen from the intercept. On average, the RH underestimation is 6.6%. When distinguishing between cropland (-8.6 %) and non-cropland (-4.1%) stations, the underestimation is more than twice as large for cropland stations. This difference can be explained by extensive irrigation in agricultural areas. Compared to the temperature bias (Figure 12), a smaller portion (31 % for all stations) of the relative humidity bias can be explained by $\Delta z_{i,j}$. This means other factors, land use being the most obvious one, influence the RH bias. Especially for cropland stations, other factors are more dominant. Only 26% of the bias can be explained by $\Delta z_{i,j}$, whereas for non-cropland stations this is 38%. An additional reason for the low R^2 for cropland stations, is that irrigation itself can be rather variable. Some stations are located in more or less intensely irrigated area and have a stronger or weaker influence on the RH bias.

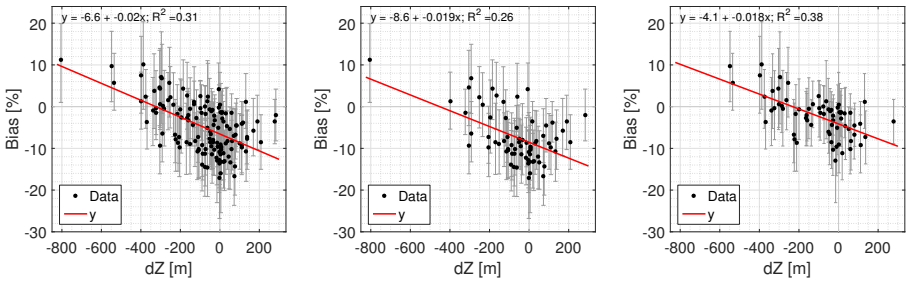

Figure 19: Relative humidity bias (GFS 2 m RH - observed RH) versus $\Delta z_{i,j}$. Left: all validation stations; middle: the 70 stations with land use 'Croplands', right: 67 non-cropland stations. Red lines denote the linear regression lines (y).

Next, I will assess the temporal variability of the performance of the GFS 2 m RH. To this end I validate the GFS relative humidity against observed relative humidity, using stations with $|\Delta z_{i,j}| < 30$ m. The bias variation throughout the day and throughout the year is given in Figure 20, separately for cropland and non-cropland stations. For all stations, the bias and its variation is smallest during day-time. GFS generally underestimates relative humidity, especially in cropland area. For croplands, this underestimation seems to increase throughout the year, until December. This suggests that GFS, assuming little or no irrigation in the area, steadily depletes soil moisture throughout the year. By that, the evaporative capacity of the land surface and consequently the relative humidity is reduced. In reality the irrigation in cropland area compensates for the soil moisture deficit, keeping the soil well-watered and evaporation not limited by water availability.

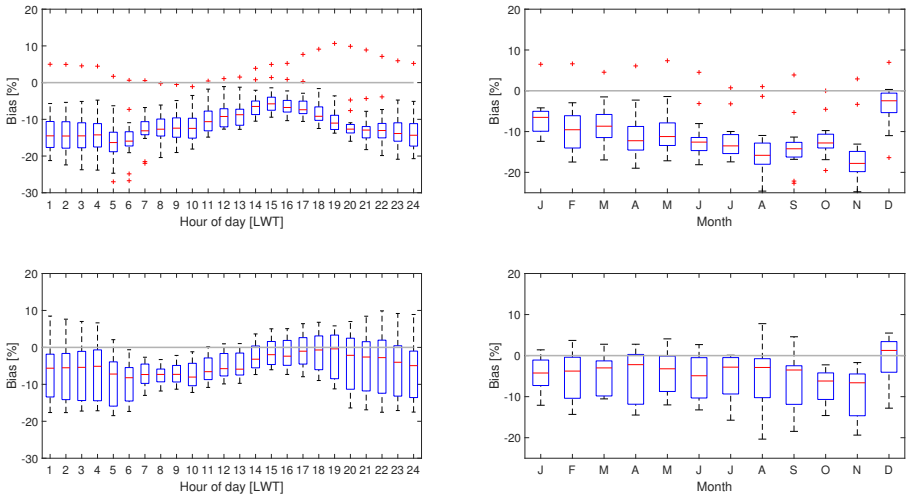

Figure 20: Bias (GFS 2 m RH - observed RH) throughout the day (left) and year (right) for stations with $|\Delta z_{i,j}| < 30$ m. Upper panel: Bias for croplands (16 stations), lower panel: Bias for non-croplands (14 stations). The hour of day is given in Local Winter Time (LWT). For each box, the central mark is the median, the edges are the 25th and 75th percentile and the whisker includes all points not considered outliers. Data beyond approximately 2.7 standard deviations from the median are considered outliers and denoted with red '+'-symbols. All data, including outliers, are shown.

4.2.2 GFS performance with downscaling

The bias of downscaled relative humidity against $\Delta z_{i,j}$ is shown in Figure 21 for all stations and separately for cropland and non-cropland stations. The systematic dry bias, which can be deducted from the intercept, is not related to $\Delta z_{i,j}$. Therefore, this dry bias remains more or less the same after downscaling. What downscaling does change, is that it eliminates the height-temperature-relative humidity relationship. This can be seen from negligibly small R^2 and regression coefficient. However, as the systematic dry error persists, the $RMSE$ does not decrease after downscaling, but remains the same at 13.7%. How this dry error affects disease modelling, for which the input of relative humidity (or related) variables is necessary, will be discussed in Section 4.4.

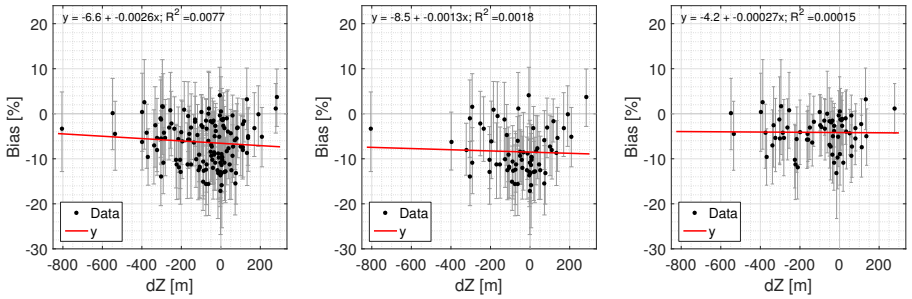

Figure 21: Relative humidity bias (GFS 2 m RH - observed RH) versus $\Delta z_{i,j}$ after downscaling using the Weighted method. Left: all validation stations; middle: the 70 stations with land use 'Croplands', right: 67 non-cropland stations. Red lines denote the linear regression lines (y).

4.3 Insect modelling

In this section I will discuss the use of either observed temperature, GFS temperature or downscaled GFS temperature using the Weighted method for insect modelling. I will do this by using the Western cherry fruit fly model as an example, but the basic principles apply to any insect model which is based solely on degree day accumulation. The empirical model is outlined in Section 3.2.1.

An example for the degree day (DD) accumulation for a station which is located in a relatively low position is given in Figure 22. With a $\Delta z_{i,j}$ of -805 m this is, compared to the GFS grid, the lowest of all stations. The relatively low position of the station leads to a systematic cold bias when using the original GFS 2 m temperature. This reduces the modelled rate of degree day accumulation. As this is a systematic error the DD difference between observed and GFS$_{orig}$ increases with a near-constant rate. When looking at fixed DD accumulations, the difference in time it takes to reach a certain amount of degree days (Δt_{DD}) increases with increasing DD. However, this also largely depends the weather: a warm spell in the first half of June increased the DD accumulation rate, as can be seen from the increasing steepness of GFS$_{Orig}$. This decreased the Δt_{DD}. The example shown here thus gives Δt_{DD} that are specific for the year of 2016, but may vary from year to year.

The timing of pest management is based upon the modelled DD accumulation of insect models. Therefore, it is very important for the timing error to be reduced to a minimum. The Western cherry fruit fly is most harmful after the egg hatch of larvae, as larvae bore into the cherries. The first eggs hatch after 594 DD have been accumulated, which for this exemplary location occurred on May 15 according to observations. Using the original, non-downscaled GFS data this amount has only been accumulated on June 26, more than one month too late. Applying downscaling reduces the Δt_{DD} to a mere 3 days. The example shown here is based on egg hatch prediction for a relatively low position. When downscaling to a sub-grid where $\Delta z_{i,j} > 0$ m, not applying downscaling will result in a too early prediction of egg hatch.

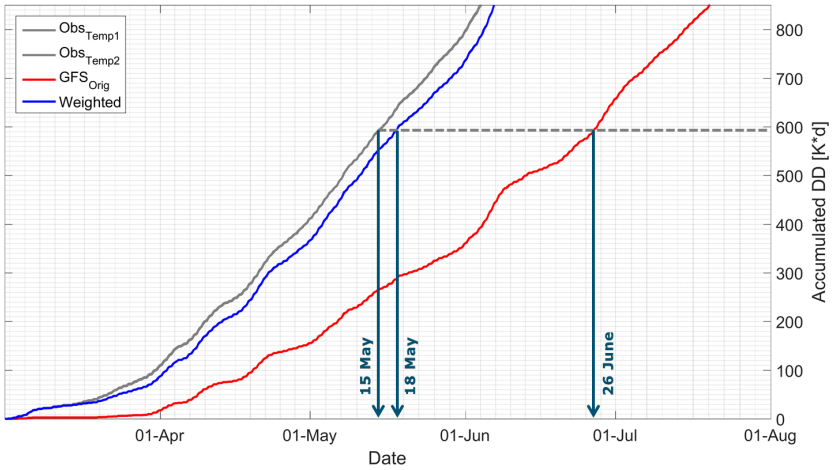

Figure 22: Degree Day accumulation since March 1 for station 'Malaga', with a $\Delta z_{i,j}$ of -805 m. Degree days are accumulated using the observed (grey), original GFS temperature (red) or downscaled GFS temperature using the Weighted method (blue).

The previous example showed the improvement of DD accumulation when the $\Delta z_{i,j}$ was large. However, when the $\Delta z_{i,j}$ is relatively small, timing uncertainties originate relatively more from factors other then elevation differences. An example of this is shown in Figure 23. For this sub-grid, with a $\Delta z_{i,j}$ of -87 m, there is a strong warm bias, especially at night. This is common for croplands (Figure 15). Applying downscaling will add to this pre-existing warm bias as the sub-grid is located lower than the GFS grid. For this station, downscaling leads to an egg hatch timing error of 7 days. When using the uncorrected GFS data, this error would have been smaller with only 4 days.

Figure 22 and 23 were two examples of how downscaling influences the timing prediction of the egg hatch. In Figure 24 we generalise that GFS is systematically too cold in regions located in a relatively low position and vice versa. This produces a systematic error in the predicted timing of egg hatch. For every 100 m of $\Delta z_{i,j}$, the timing is 5 days off. In an optimal situation, where farmers have on-site weather stations, the average timing error caused by measurement

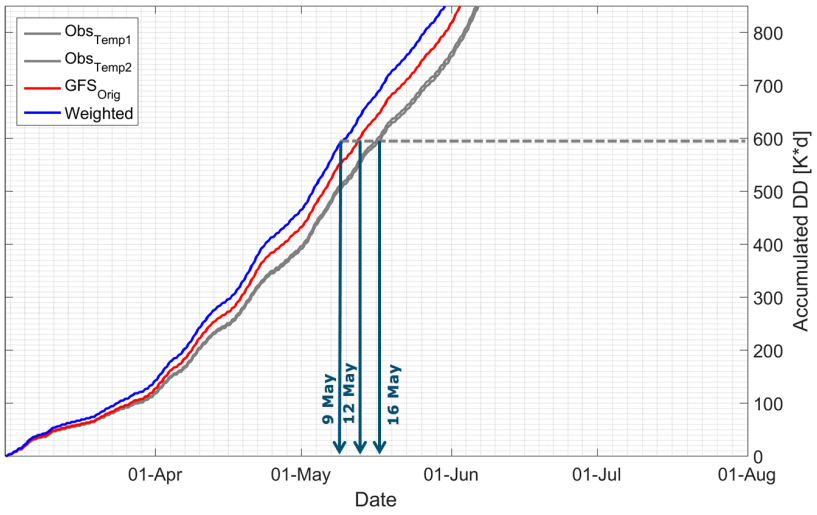

Figure 23: Degree Day accumulation since March 1 for station 'Mc Nary', with a $\Delta z_{i,j}$ of -87 m. Degree days are accumulated using the observed (grey), original GFS temperature (red) or downscaled GFS temperature using the Weighted method (blue).

errors of the equipment is 0.7 ± 1.3 days. I estimated this measurement error from the differences between thermometer 1 and 2. When there are no on-site weather stations, using downscaled GFS temperature gives a mean timing error of 0.2 ± 6 days.

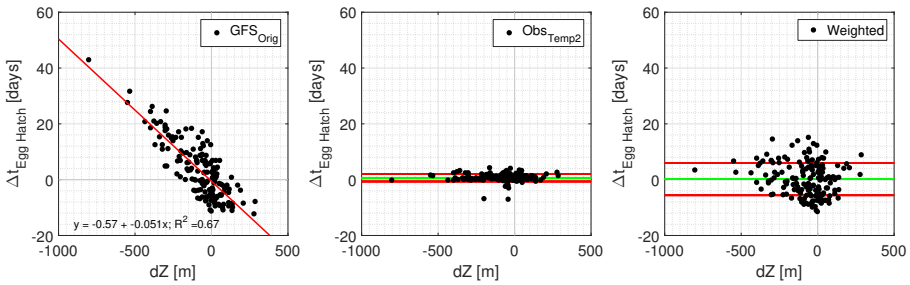

Figure 24: Difference in timing of predicted egg hatch compared to egg hatch timing using thermometer 1. A positive Δt denotes a delayed predicted egg hatch timing. Left: Δt using the original GFS 2m temperature; middle: Δt using thermometer 2; right: Δt using the downscaled (applying the Weighted method) 2m temperature.

Overall, in mountainous areas downscaling the GFS 2 m temperature greatly improves the accuracy of the predicted timing of developmental transitions compared to using uncorrected GFS data. The average timing error is less than a day with a standard deviation of less than a week. This makes using downscaled GFS 2 m temperature for simple insect models very attractive, especially in areas without on-site weather stations. For areas which do have on-site weather stations, as in Washington State, the forecast temperature may be used to predict when certain amounts of degree days will be accumulated. Downscaling temperatures forecast for more than +3 hours ahead is not investigated in this thesis. However, I expect that applying downscaling will significantly improve the accuracy of the predicted timing compared to using uncorrected GFS forecasts.

4.4 Disease modelling

To demonstrate the sensitivity of disease models to the quality of the weather data I used an adapted version the Late Blight model by Ullrich and Schrödter (1966). A full model description can be found in Section 4.4. In short, a high relative humidity and a favourable temperature increase the risk for Late Blight. As GFS systematically underestimates relative humidity, using GFS data will likely cause an underestimation of the risk for plant diseases.

For every cropland sub-grid and for each week of the year, a risk value (RV) is calculated. Figure 25 shows the RVs that have been accumulated as a function of weekly average temperature and relative humidity. RV was calculated using either observations, uncorrected and corrected GFS data. For clarity, the size of the dots are scaled with the risk value. It becomes clear that even though the blight model is bimodal, there is a strong preference for a high RV when weekly averaged temperature is around 10 to 12 degrees. The model's second mode around 21 degrees does not show from the risk values. This can only be because at higher temperatures (prolonged) saturation is less likely to occur. It is also interesting to note that in general risk values are low, as the disease is expected at risk values higher than 150. Using the GFS data, both uncorrected and downscaled, leads to an underestimation of the occurrence of relatively high risk values. As the strong systematic dry error of GFS is not resolved by downscaling the risk values are underestimated and therefore both GFS scatterplots do not show clear differences.

When looking at how the RV develops throughout the year (Figure 26) it can be seen that the average RV is relatively low, by far not reaching the action threshold of 150. The spring and autumn season have the highest average RV, which may be explained by a combination of favourable temperatures and not yet too low relative humidity, which is the reason for the 'dip' in summer. The winter period shows on average the lowest RV values. In this case the relative humidity is not the limiting factor, but the low temperature.

This then raises the question which parts of the region are the most vulnerable for Late Blight. Figure 27 shows for each station the highest RV that occurred in the whole year of 2016. Again, shown are the RV calculated from observations, uncorrected and corrected GFS data. Highest RV clearly occur in

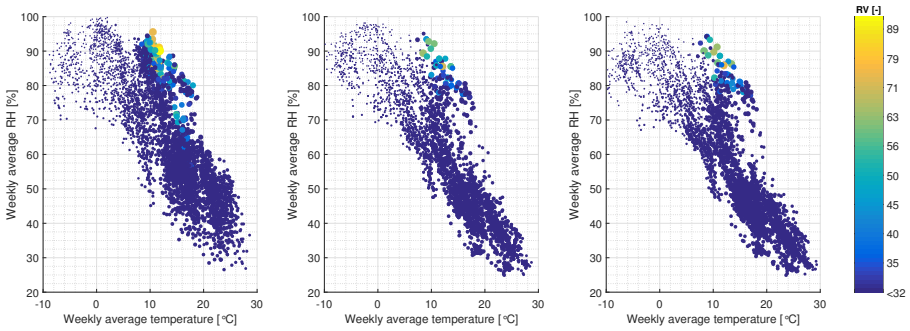

Figure 25: Colour plots of weekly accumulated Late Blight risk values (RV) as a function of weekly averaged temperature and humidity for cropland stations. The risk values are calculated using observations (left), uncorrected (middle) or corrected GFS data using the Weighted method (right). Each dot represents one RV value for one station, in total there are 81 cropland stations with 52 risk values each. Note that dots may overlap. The size and colour of each dot is scaled to the risk value. As you can start to accumulate the RV on each arbitrary day of the week, the RV may be higher or lower depending on the start date. RVs shown here are, for every starting day, the highest RVs obtained weekly.

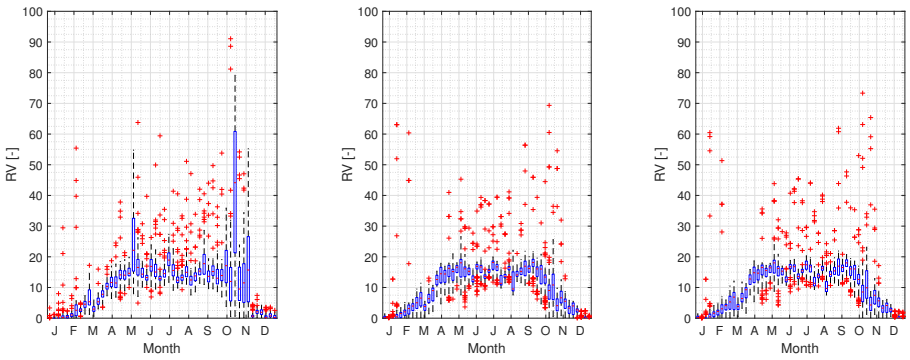

Figure 26: Boxplot of the development of the Late Blight risk value (RV) throughout the year for cropland stations. Risk values are accumulated on a weekly basis. The risk values are calculated using observations (left), uncorrected (middle) or corrected GFS data using the Weighted method (right). The boxplot shows the spatial variation of 81 cropland stations stations. Red crosses denote outliers.

the marine region. This is also picked up quite well by GFS. The high RV in the marine region has a simple explanation: not only is the relative humidity high due to moisture advection from the sea, but temperatures are mild and 'blight-friendly' during winter. This is also depicted by the GFS model. What GFS does not depict at all is the high RV in the plateau region. Climatologically this is a very dry region with a low relative humidity. However, water is added to the system through irrigation raising the relative humidity. This will be further discussed in Section 5.

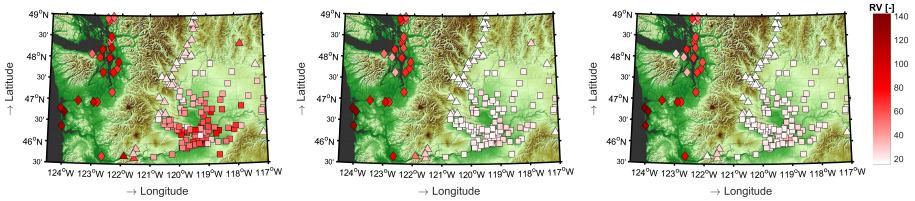

Figure 27: Spatial distribution of the yearly maximum Late Blight risk value (RV). The risk values are calculated using observations (left), uncorrected (middle) or corrected GFS data using the Weighted method (right).

Concluding, GFS can certainly be useful for depicting relatively high RVs where conditions are favourable to due large scale phenomena such as moist air advection and mild winter temperatures in marine regions. However, if favourable conditions stem from irrigation GFS completely misses the increased risk for plant diseases such as Late Blight.

5 Discussion

I have investigated how sensitive disease and pest models are to the accuracy of the meteorological data input. To do this I have first validated uncorrected and corrected GFS analysis and forecast data using stations in Washington State. Stations which are biased to being situated in (the vicinity of) crop fields. I have drawn conclusions on the performance of GFS based on these biased met-stations. Validating GFS in undisturbed areas, or validating using an un-biased network may have resulted in a different GFS accuracy. Fact is, however, the application of these pest and disease models will be biased toward croplands.

I have used several methodologies for the topography-based downscaling of GFS air temperature. The decreased temperature bias and $RMSE$ showed that downscaling significantly improved the accuracy of the GFS 2 m temperature. My results have shown that the Weighted method was one of the most robust and reliable method for downscaling air temperature. However, using model-internal lapse rates did not significantly improve the accuracy more than simply using a fixed lapse rate of -6.5 °C/km. $RMSE$ differences among downscaling methods did not exceed 0.1 °C. This is opposed to the results of Gao et al. (2012), who showed that model-internal lapse rates resulted in a $RMSE$ that was 34% lower compared to literature-based lapse rates. However, the network of stations he used was very different. Gao et al. (2012) validated his downscaling method using 12 stations which were on average positioned 360 m higher than the height of the ERA-interim grid cell. In Washington State, the meteorological stations were on average positioned only 77 m lower than the GFS elevation. It would be very interesting to see which of the downscaling methods of this research performs best when $\Delta z_{i,j}$ are more extreme.

By downscaling based on a DEM, I assumed elevation differences as being the dominant factor in determining the bias of GFS. However, local phenomena can also be a cause for the systematic discrepancy between GFS and observed temperature and relative humidity. This is likely an issue of irrigation not being

represented well enough in the current GFS land surface model. A summertime warm and dry bias has been previously observed over the Great Plains and was followed by a correction of grassland and cropland surface characteristics in the land surface model used by GFS (American Meteorological Society, 2017). A similar improvement may have to implemented in the North-West of the US. This is further substantiated by ample evidence of the weather-related impacts of irrigation: cooling in the dry season (Kueppers et al., 2007), a shifting partitioning of the surface energy fluxes towards significantly more latent heat flux (de Rosnay et al., 2003; Haddeland et al., 2006) and increases in relative humidity (Kueppers et al., 2008). Even the night-time warm bias in croplands observed in this thesis is very likely to be related to irrigation. Kanamaru and Kanamitsu (2008) showed that irrigated, and thus wetter, soils reduce night-time surface cooling due to an increase of the ground heat flux. This increased ground heat flux is caused by an increased thermal conductivity of wet soils. Next to the representation of irrigation other local phenomena are not well represented. In or near urban areas, even as extensive as Seattle and Vancouver, the observed urban heat island effect is not modelled by GFS. In addition, topography-related phenomena such as drainage flow at night, or sun-facing slope aspects that warm faster may be too coarse a phenomena for GFS.

In this research I have shown the application of two very simple insect and disease models which were solely based on temperature and relative humidity. Much more complex models do exist, but these simple, empirical models have been, for a long time, widely applied and extensively validated. Requiring only a limited amount of data this is a cheap way to monitor insect and disease risk. Being rather simple, one should always be aware when applying these empirical insect and disease models in climates other than those where the model has been validated for. The same species may develop differently in other climates. Despite these uncertainties, the concepts underlying insect and disease models are the same: favourable weather conditions lead to a higher risk. This is why I justify my generalised interpretation or my results. Even though the results were acquired based on the application of only two models, the risk values of which I only validated in one specific region.

In the end, for insect and disease modelling it is mainly important for the error that is left after downscaling not to be biased. For insect modelling, downscaling temperature based on elevation is sufficient for obtaining an accurate indication of the accumulated degree days, with an uncertainty of more or less a week. Concerning disease modelling, the GFS dry bias leads to a systematic underestimation of the risk for plant diseases in the agricultural area situated on the Columbian Plateau. The original Late Blight model used in this study also incorporated a rainfall threshold, whereas I have only solely used the relative humidity threshold. When incorporating rainfall, risk values will be higher as the conditions for an (increased) risk value accumulation are more often met. However, for the Columbian Plateau I do not expect the effect of including rainfall will be large, as rainfall in this area is scarce.

As mentioned, corrected GFS data are suitable for insect modelling. This is especially useful in areas where no (reliable) observations are available. However, also in well-monitored areas using GFS data can be useful. I have not

investigated the accuracy of forecasts of more than 3 hours ahead, but these could be used to make a prediction of degree day accumulation. Not only can downscaled temperature data be used for insect modelling but in other fields it may provide a useful application, such as hydrologic modelling (Praskievicz and Bartlein, 2014; Hay and Clark, 2003) snow-melt modelling (Sen Gupta and Tarboton, 2016) and downscaling climate change scenarios (Pierce et al., 2013).

6 Conclusion

There is a need for systems that can alarm farmers on the risk of insect pest and plant diseases. Simple models exist that predict the risk for pest and diseases based on weather variables. However, meteorological stations may not be present, or are unreliable. I have investigated whether freely available GFS data can be used to provide temperature and relative humidity data used in such models. In mountainous areas, GFS data are however too coarse for field-scale modelling, as weather changes rapidly with height.

I have investigated several downscaling methods for obtaining temperature and relative humidity fields with a higher spatial resolution. These downscaling methods were based on different techniques to define the lapse rate, which I use to downscale temperature based on a high resolution digital elevation map. Usually, a fixed lapse rate of -6.5 °C/km is applied. However, in reality the lapse rate is temporally and spatially variable. Using a model-internal lapse rate, obtained from the vertical temperature profile within GFS, the lapse rate is allowed to vary in time and space. All methods managed to significantly decrease the bias of GFS temperature and thereby improved the accuracy of the GFS temperature data. Out of the downscaling method tested, the Weighted method was shown be the most reliable considering both the reduction in root mean squared error as well as being robust and reliable. The Weighted methods considers an extensive air column. Using statistics, the eventual lapse rate is then calculated from a weighted average lapse rate of the air column at a specific time and place.

Downscaling relative humidity was done assuming the specific humidity to be conserved, which is true when the air mass composition is unchanged moving up or down to the desired sub-grid. Downscaling based on elevation did indeed eliminate the systematic error related to elevation differences, however a systematic dry bias remained. This dry bias was evident both cropland as well as non-cropland areas, but much stronger so in cropland. The latter can be explained by the application of irrigation, keeping the soil surface well-watered and evaporation not limited by a lack of water availability.

The downscaled temperature data show a large potential to be used for simple insect modelling which is based on degree day accumulation. This was shown by using an example of the predicted timing of the egg hatch of the Western cherry Fruit fly. Not applying downscaling results in a timing error which increases by around 5 days for every 100 meter elevation difference. Downscaling the temperature using the Weighted method resulted in an average timing error of less than a day with an uncertainty of less than a week. This uncertainty originated from temperature inaccuracies that remained after downscaling. In

areas where no observations and related data on degree day accumulation are available, downscaled GFS data can be a reliable alternative source of data.

The GFS relative humidity data show a strong dry bias, which cannot be resolved by downscaling based on elevation differences. As plant diseases rely on the availability of moisture in order to develop, the risk for diseases is underestimated. This underestimation is strongest in cropland areas, where irrigation leads to an increase in relative humidity. A likely solution to this problem is to implement, or if already present to improve, an irrigation scheme in the land surface model used by GFS. However, this will not be sufficient for areas with small-scale agriculture where the land use map used by GFS is still too coarse for depicting cropland.

The downscaling methods presented in this study and related degree day accumulation may not only be valuable for pest modelling in mountainous areas. Useful applications may be found in other fields of science, such as catchment hydrology, snow-melt modelling or downscaling climate projections.

7 Acknowledgements

First of all I want to thank AgWeatherNet for providing a year-long record of weather data for all their stations. I want to thank Sean Hill specifically for answering my questions and resolving a summertime issue. I have signed a petition hoping we will for once and for all stop using Daylight Saving Time, but so far it has been up to no avail. Perhaps in future better times will be ahead. Preferably wintertimes.

I also want to thank Grace Peng of NCAR for patiently answering my questions on the GFS model. Clarifying the geoid representation of earth helped me taking my thesis to the appropriate level [m a.s.l.]. After my relatively silly humidity inquiry I have pledged never again to make the mistake to convert variables from Kelvin to Celcius when the variable involved is not temperature.

Last but not least, I want to thank my supervisor Oscar Hartogensis for his tremendous dedication to guide my work. Our weekly meetings and more-than-weekly e-mail conversations helped me get the most out of my research. Oscar's metaphorical bread crumbs were essential ingredients to my Master Piece of Science.

Bibliography

M. T. Ali Niazee. A computerized phenology model for predicting biological events of rhageletis indifferens (diptera: Tephritidae). *The Canadian Entomologist*, 111(10):11011109, 1979. doi: 10.4039/Ent1111101-10.

American Meteorological Society. Evaluation of the May 2016 GFS Upgrade. `https://ams.confex.com/ams/97Annual/webprogram/Paper313166.html`, 2017.

E. Bursell. Environmental aspects: temperature. *The physiology of Insecta*, 1: 283–321, 1964.

Central Intelligence Agency. The world factbook - bolivia. `https://www.cia.gov/library/publications/the-world-factbook/geos/bl.html`, December 2015.

P. de Rosnay, J. Polcher, K. Laval, and M. Sabre. Integrated parameterization of irrigation in the land surface model orchidee. validation over indian peninsula. *Geophysical Research Letters*, 30(19), 2003. ISSN 1944-8007. doi: 10.1029/2003GL018024.

Food and A. O. of the United Nations. *The State of Food and Agriculture 2001*. Number 33. Food & Agriculture Org., 2001.

M. A. Friedl, D. Sulla-Menashe, B. Tan, A. Schneider, N. Ramankutty, A. Sibley, and X. Huang. Modis collection 5 global land cover: Algorithm refinements and characterization of new datasets. *Remote Sensing of Environment*, 114 (1):168–182, 2010.

L. Gao, M. Bernhardt, and K. Schulz. Elevation correction of era-interim temperature data in complex terrain. *Hydrology and Earth System Sciences*, 16 (12):4661–4673, 2012. doi: 10.5194/hess-16-4661-2012.

Google Earth. Topographical map of Washington State, USA, 2017. V 7.1.8.3036.

I. Haddeland, D. P. Lettenmaier, and T. Skaugen. Effects of irrigation on the water and energy balances of the colorado and mekong river basins. *Journal of Hydrology*, 324(1):210 – 223, 2006. ISSN 0022-1694. doi: http://dx.doi.org/10.1016/j.jhydrol.2005.09.028.

L. Hay and M. Clark. Use of statistically and dynamically downscaled atmospheric model output for hydrologic simulations in three mountainous basins in the western United States. *JOURNAL OF HYDROLOGY*, 282(1-4):56–75, NOV 10 2003. ISSN 0022-1694. doi: {10.1016/S0022-1694(03)00252-X}.

H. Kanamaru and M. Kanamitsu. Model diagnosis of nighttime minimum temperature warming during summer due to irrigation in the california central valley. *Journal of Hydrometeorology*, 9(5):1061–1072, 2008. doi: 10.1175/2008JHM967.1.

L. M. Kueppers, M. A. Snyder, and L. C. Sloan. Irrigation cooling effect: Regional climate forcing by land-use change. *Geophysical Research Letters*, 34(3), 2007. ISSN 1944-8007. doi: 10.1029/2006GL028679. L03703.

L. M. Kueppers, M. A. Snyder, L. C. Sloan, D. Cayan, J. Jin, H. Kanamaru, M. Kanamitsu, N. L. Miller, M. Tyree, H. Du, and B. Weare. Seasonal temperature responses to land-use change in the western united states. *Global and Planetary Change*, 60(3):250 – 264, 2008. ISSN 0921-8181. doi: http://dx.doi.org/10.1016/j.gloplacha.2007.03.005.

K. Kunkel. Simple procedures for extrapolation of humidity variables in the mountainous western united states. *Journal of Climate*, 2:656–669, 1988.

D. Ludwig. The effects of temperature on the development of an insect (popillia japonica newman). *Physiological Zoology*, 1(3):358–389, 1928.

J. D. Lundquist and D. R. Cayan. Surface temperature patterns in complex terrain: Daily variations and long-term change in the central sierra nevada, california. *Journal of Geophysical Research: Atmospheres*, 112(D11):1–15, 2007. ISSN 2156-2202. doi: 10.1029/2006JD007561. D11124.

E. Maurer, A. Wood, J. Adam, D. Lettenmaier, and B. Nijssen. A long-term hydrologically based dataset of land surface fluxes and states for the conterminous united states. *Journal of Climate*, 15(22):3237–3251, 2002. cited By 662.

A. F. Moene and J. C. van Dam. *Transport in the Atmosphere-Vegetation-Soil Continuum*. Cambridge University Press, 1 edition, 2014. ISBN 9780521195683.

NASA JPL. ASTER Global Digital Elevation Model V002 . `https://lpdaac.usgs.gov/node/1079`, 2009.

National Centers for Environmental Prediction. NCEP GDAS/FNL 0.25 Degree Global Tropospheric Analyses and Forecast Grids. https://doi.org/10.5065/D65Q4T4Z, 2015.

T. R. Oke. The energetic basis of the urban heat island. *Quarterly Journal of the Royal Meteorological Society*, 108(455):1–24, 1982.

G. Peng. What's the difference between GFS and FNL? http://ncarrda.blogspot.nl/2015/04/whats-difference-between-gfs-and-fnl.html, April 2015.

D. W. Pierce, T. Das, D. R. Cayan, E. P. Maurer, N. L. Miller, Y. Bao, M. Kanamitsu, K. Yoshimura, M. A. Snyder, L. C. Sloan, G. Franco, and M. Tyree. Probabilistic estimates of future changes in California temperature and precipitation using statistical and dynamical downscaling. *CLIMATE DYNAMICS*, 40(3-4):839–856, FEB 2013. doi: {10.1007/s00382-012-1337-9}.

S. Praskievicz and P. Bartlein. Hydrologic modeling using elevationally adjusted NARR and NARCCAP regional climate-model simulations: Tucannon River, Washington. *JOURNAL OF HYDROLOGY*, 517:803–814, SEP 19 2014. doi: {10.1016/j.jhydrol.2014.06.017}.

B. Ratner. *Upper-air climatology of the United States. Part 1: Averages for isobaric surfaces, height, temperature, humidity and density.* U.S. Department of Commerce Weather Bureau, 1957.

C. Rosenzweig, A. Iglesias, X. Yang, P. R. Epstein, and E. Chivian. Climate change and extreme weather events; implications for food production, plant diseases, and pests. *Global Change and Human Health*, 2(2):90–104, 2001. ISSN 1573-7314. doi: 10.1023/A:1015086831467. URL http://dx.doi.org/10.1023/A:1015086831467.

S. Sankaran, A. Mishra, R. Ehsani, and C. Davis. A review of advanced techniques for detecting plant diseases. *Computers and Electronics in Agriculture*, 72(1):1 – 13, 2010. ISSN 0168-1699. doi: http://dx.doi.org/10.1016/j.compag.2010.02.007. URL http://www.sciencedirect.com/science/article/pii/S0168169910000438.

A. Sen Gupta and D. G. Tarboton. A tool for downscaling weather data from large-grid reanalysis products to finer spatial scales for distributed hydrological applications. *ENVIRONMENTAL MODELLING & SOFTWARE*, 84: 50–69, OCT 2016. doi: {10.1016/j.envsoft.2016.06.014}.

K. Stahl, R. Moore, J. Floyer, M. Asplin, and I. McKendry. Comparison of approaches for spatial interpolation of daily air temperature in a large region with complex topography and highly variable station density. *Agricultural and Forest Meteorology*, 139(3-4):224–236, 2006. doi: 10.1016/j.agrformet.2006.07.004. cited By 126.

H. E. Tonnang, B. D. Herv, L. Biber-Freudenberger, D. Salifu, S. Subramanian, V. B. Ngowi, R. Y. Guimapi, B. Anani, F. M. Kakmeni, H. Affognon, S. Niassy, T. Landmann, F. T. Ndjomatchoua, S. A. Pedro, T. Johansson, C. M. Tanga, P. Nana, K. M. Fiaboe, S. F. Mohamed, N. K. Maniania, L. V.

Nedorezov, S. Ekesi, and C. Borgemeister. Advances in crop insect modelling methodstowards a whole system approach. *Ecological Modelling*, 354:88 – 103, 2017. ISSN 0304-3800. doi: http://dx.doi.org/10.1016/j.ecolmodel.2017.03.015.

UCAR. Washington State: Average Annual Precipitation 1961-1990. `https://www.meted.ucar.edu/search/details.php?id=11937`, 2017.

J. Ullrich and H. Schrödter. Das problem der vorhersage des auftretens der kartoffelkrautfäule (phytophthora infestans) und die möglichkeit seiner lösung durch eine negativprognose. *Nachrichtenblatt Deutsch. Pflanzenschutzdienst (Braunschweig)*, 18:33–40, 1966.

University of California. About phenology models. `http://ipm.ucanr.edu/`, June 2016.

J. S. West, J. A. Townsend, M. Stevens, and B. D. L. Fitt. Comparative biology of different plant pathogens to estimate effects of climate change on crop diseases in europe. *European Journal of Plant Pathology*, 133(1):315–331, 2012. ISSN 1573-8469. doi: 10.1007/s10658-011-9932-x. URL `http://dx.doi.org/10.1007/s10658-011-9932-x`.

WSU. AgWeatherNet. `http://weather.wsu.edu`, 2017.